RESEARCH ARTICLE

Fusion-based approach for hydrometeorological drought modeling: a regional investigation for Iran

Fatemeh Moghaddasi[1] · Mahnoosh Moghaddasi[1,2] · Mehdi Mohammadi Ghaleni[1,2] · Zaher Mundher Yaseen[3,4]

Abstract

The objective of this study was to model a new drought index called the Fusion-based Hydrological Meteorological Drought Index (FHMDI) to simultaneously monitor hydrological and meteorological drought. Aiming to estimate drought more accurately, local measurements were classified into various clusters using the AGNES clustering algorithm. Four single artificial intelligence (SAI) models—namely, Gaussian Process Regression (GPR), Ensemble, Feedforward Neural Networks (FNN), and Support Vector Regression (SVR)—were developed for each cluster. To promote the results of single of products and models, four fusion-based approaches, namely, Wavelet-Based (WB), Weighted Majority Voting (WMV), Extended Kalman Filter (EKF), and Entropy Weight (EW) methods, were used to estimate FHMDI in different time scales, precipitation, and runoff. The performance of single and combined products and models was assessed through statistical error metrics, such as Kling–Gupta efficiency (KGE), Mean Bias Error (MBE), and Normalized Root Mean Square Error (NRMSE). The performance of the proposed methodology was tested over 24 main river basins in Iran. The validation results of the FHMDI (the compliance of the index with the pre-existing drought index) revealed that it accurately identified drought conditions. The results indicated that individual products performed well in some river basins, while fusion-based models improved dataset accuracy more compared to local measurements. The WMV with the highest accuracy (lowest NRMSE) had a good performance in 60% of the cases compared to all other products and fusion-based models. WMV also showed higher efficiency in 100% of the cases than all other fusion-based and SAI models for simultaneous hydrological and meteorological drought estimation. In light of these findings, we recommend the use of fusion-based approach to improve drought modeling.

✉ Mahnoosh Moghaddasi
m-moghaddasi@araku.ac.ir

1   Department of Water Science and Engineering, Faculty of Agriculture and Environment, Arak University, Arak, Iran

2   Research Institute for Water Science and Engineering, Arak University, Arak, Iran

3   Civil and Environmental Engineering Department, King Fahd University of Petroleum & Minerals, 31261 Dhahran, Saudi Arabia

4   Interdisciplinary Research Center for Membranes and Water Security, King Fahd University of Petroleum & Minerals, 31261 Dhahran, Saudi Arabia

Introduction

Drought is a periodic natural hazard that negatively influences water resources (Nemati et al. 2019; Scanlon et al. 2017). This phenomenon is typically divided into different categories in terms of water deficit type, including hydrological that occurs when surface and subsurface water levels are significantly below normal (Barker et al. 2016), agricultural which considers soil moisture deficiency (Yan et al. 2017), socio-economical that accounts for water resources system deficit resulting from other types of drought (Huang et al. 2016), and meteorological droughts which account for precipitation shortage (Hameed et al. 2018). Hydrological drought is generally caused by an uninterrupted meteorological drought (Wu et al. 2017) with various effects on the economy, agriculture, and ecology, including reduced hydraulic power production and irrigation water supply

(Mishra and Singh 2010). In other words, various types of droughts can occur at the same time, making it difficult to distinguish between them. As a result, univariate drought indices (rely on single variable) are insufficient for characterizing the complicated effects and conditions of droughts, and composite indices have been suggested to overcome this difficulty (Yang et al. 2018). Therefore, it is necessary to have efficient indices to simultaneously monitor hydrological and meteorological droughts.

In recent years, researchers have tried to introduce new multivariate indices by combining drought indices using various methods to gain more information on the features and situation of this climatic phenomenon (Fahimirad and Shahkarami 2021; Li et al. 2014; Motevali Bashi Naeini et al. 2021; Nazeri Tahroudi et al. 2020; Hosseini et al. 2023).

Numerous current research efforts have monitored and analyzed the types of droughts using interpolated grids or observational data (Henriques and Santos 1999; Santos et al. 2010; Shen and Tabios 1995). Meteorological hydrometric stations can monitor variabilities in precipitation and runoff and accurately estimate precipitation and hydrological fluxes across basins (Fekete et al. 2002). But, there are few or no stations in specific locations worldwide due to the high cost of gauge installation and maintenance, and the existing records may be lacking or related to smaller time frames (Salio et al. 2015; Sun et al. 2018). To overcome the data scarcity in developing regions, alternative sources of global gridded datasets have been developed by different institutions—such as Modern-Era Retrospective Analysis for Research and Applications (Rienecker et al. 2011) and Global Land Data Assimilation System (Rodell et al. 2004)—that benefit the monitoring of water resources in regions with no or poor gauge systems. Each dataset offers certain advantages concerning the provided variables, temporal and spatial resolution, geographic extent, and time period. The gridded datasets were divided into three categories: namely, reanalysis, satellite-based, and gauge-based products (Hosseini-Moghari et al. 2018; Saemian et al. 2022). The reanalysis products assimilate remote sensing and in situ observations as numerical models of the global atmosphere and land surface (Dee et al. 2011; Saha et al. 2010). Estimations provided by these datasets are used for many research and applied cases, such as trend analysis (Balling et al. 2016; Toride et al. 2018), drought monitoring (Ahmadebrahimpour et al. 2019; Golian et al. 2019; Liu et al. 2020), flood modeling (Dis et al. 2016; Nhi et al. 2018; Yuan et al. 2019), and stream-flow simulation (Try et al. 2020; Yuan et al. 2017).

Droughts can be predicted using various models, for example, data-driven models (Dikshit and Pradhan 2021; Park et al. 2017; Zhang et al. 2019; Nejatian et al. 2023), autoregressive integrated moving average (Mishra and Desai

2006, 2005), Markov Chain (Alam et al. 2014; Rahmat et al. 2017), and hydrological (e.g., (Trambauer et al. 2013; Xing et al. 2020). However, as is the case with the rest of the statistical and linear models, complex drought conditions cannot be predicted by single data-driven models. Multi-model combination/fusion-based method, as a new approach, improves the credibility of data-driven models and resolves their shortcomings. Drought can be assessed through fusion more accurately than models based on single data sources. This approach was proposed by Dasarathy (1997), and it allows for gaining greater insight than single data sources. This method has been employed for streamflow forecasting (Modaresi et al. 2018), river-level forecasting (See and Abrahart 2001), and flood frequency analysis (ensemble model) (Shu and Burn 2004). This approach can predict drought by merging single forecasts. It has been suggested that combining remotely sensed datasets provides better forecasts than in-situ observations (Feng et al. 2019; Fooladi et al. 2021; Jiao et al. 2019; Park et al. 2017). A review of the previous research showed that various single artificial intelligence (SAI) models have been employed for drought modeling (Jalalkamali et al. 2015; Naderi et al. 2022). Meanwhile, fusion-based methods have outperformed single-modal methods in drought modeling.

Previous studies mostly focused on the evaluation and validation of various precipitation products worldwide (Rahmati Ziveh et al. 2022; Raziei and Sotoudeh 2017), whereas runoff products were validated in very limited regions (Qi et al. 2020). Meanwhile, few studies have directly investigated the application of fusion-based methods in fusing multiple datasets to improve runoff and precipitation trend assessment compared to in-situ measurements (Fooladi et al. 2023) and to promote accuracy, reliability, and stability of SAIs (Alizadeh and Nikoo 2018).

Therefore, the overall aim of this study is to fill this gap by assessing and inter-comparing various precipitation and runoff gridded products through gauge observation and fusion-based methodologies to model meteorological and hydrological drought in 24 large river basins in Iran. Different gridded precipitation and runoff products were employed to estimate Non-Parametric Standardized Precipitation Index (NSPI) and Non-Parametric Standardized Runoff Index (NSRI) as meteorological and hydrological drought indices, respectively, against local observations. The new composite drought index namely the Fusion-based Hydro-Meteorological Drought Index (FHMDI) was developed which is composed of the mentioned indices. In this case, four SAI models—including Support Vector Regression (SVR), Ensemble, Gaussian Process Regression (GPR), and Feedforward Neural Networks (FNN)—were used to estimate FHMDI in different time scales. Considering the different accuracy of SAI models, four fusion-based methods—namely, Wavelet-Based (WB), Weighted Majority

Voting (WMV), Extended Kalman Filter (EKF), and Entropy Weight (EW)—were applied to improve the results of SAIs. Overall, the research objectives are to:

(i) Assessing multiple remotely sensed monthly runoff and precipitation datasets individually, as well as employing a fusion-based approach including WB, EKF, WMV, and EW to evaluate multi-source runoff and precipitation remote sensing datasets, in order to enhance estimation accuracy

(ii) Calculate the FHMDI compound drought index in simultaneous hydrological and meteorological drought estimations at different time scales using various gridded products and compare the results with ground-based FHMDI

(iii) Compare four SAI models including Ensemble, GPR, FNN, and SVR in estimating FHMDI with remote sensing datasets under six scenarios (model input selection) and employing a fusion-based approach including WB, EKF, WMV, and EW to improve the accuracy combined drought estimation

The rest of the paper is organized as follows: "Material and methods" briefly describes the study area datasets and the methodology used for the study, "Results" discusses the results, "Discussion" provides discussion, and "Conclusion" presents conclusions.

Material and methods

Study area

Iran is located in the southwest of Asia with an area of about 1.7 million km^2 (Fig. 1). About 60% of the country is covered by two mountain ranges: the Zagros range extends southward from the northwest to the shores of the Persian Gulf, while the Alborz chain extends from the northwest to the northeast along the southern edge of the Caspian Sea. The elevation of Iran ranges from less than -297 m at the Caspian sea to 5597 m in the Damavand peak of Alborz Mountain chain. Precipitation values in Iran are also very diverse so that the average annual precipitation during the study varied from 52.6 mm at Zabol station to 1694.7 mm at Anzali station. Also, mean annual runoff is on average among the basins about 39 mm, but is much lower, 0–25 mm, in 18 of the 30 basins (Moshir Panahi et al. 2020). Iran has six main water basins and 30 river basins. Table 1

Fig. 1 Location of river basins and their synoptic and hydrometric stations across Iran
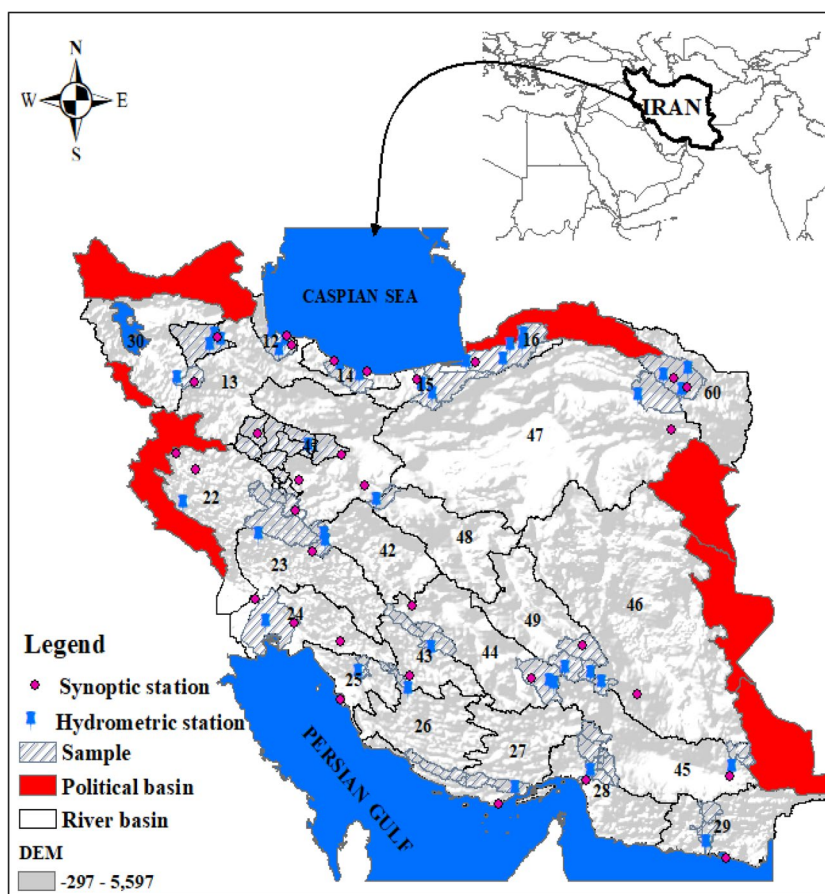
Table 1 General information on main river basins, their area, and selected synoptic and hydrometric stations

Code	River basins	Area (10³ km^2)	Synoptic station			Hydrometric station		
			Name	X	Y	Name	X	Y
28	**Bandar Abbas**	41	Minab	57.08	27.1	Minab	51.19	37.38
45	**Hamun-Jazmurian**	64	Iranshahr	60.7	27.2	Daman	60.78	30.18
49	**Daranjir-Saghand**	48	Kerman	56.96	30.25	Daranji	51.17	29.56
27	**Kol-Mehran**	58	Bandarlenge	54.83	26.53	Dezhgan	55.27	38.03
29	**South Baluchestan**	44	Chabahar	60.61	25.28	Kahir	60.13	36.86
48	**Siahkooh**	47	Kashan	51.45	33.98	Polhanjen	51.76	33.61
46	**Lut Desert**	195	Bam	58.35	29.1	Mar Sorakh	57.46	29.34
26	**Mand**	44	Shiraz	52.6	29.53	Bandbahman	52.56	27.75
25	**Helle**	20	Bushehr and Dogon-badan	50.83 and 50.81	28.98 and 30.34	Chitiborki	51.3	27.5
24	**Jarahi and Zohreh**	38	Omidieh and Ahwaz	49.66 and 48.66	30.76 and 31.33	Gargar	48.95	29
47	**Central Desert**	224	Torbat Heydarieh	59.21	35.26	Hoseinabadjangal	58.38	35.04
41	**Lake Namak**	91	Ghom and Hamedan and Arak	50.85 and 48.71 and 49.76	34.7 and 35.2 and 34.1	Jalayer	50.04	34.89
44	**Abarghoo-Sirjan**	54	Sirjan	55.68	29.46	Sirjan	56.13	30.7
60	**Ghareghoom**	44	Mashhad and Ghol-makan	59.63 and 59.28	36.26 and 36.48	Moshang	59.03	36.51
43	**Tashk Bakhtegan**	29	Abadeh	52.66	31.18	Tangbolagh	53.15	31.63
42	**Gavkhuni**	40	Koohrang	50.11	32.43	Ghale shahrokh	50.46	29.82
16	**Gharesou Gorgan**	15	Gorgan	54.26	36.85	Gorgan	55.50	37.48
30	**Lake Urmia**	53	Takab	47.11	36.38	Safakhane	46.70	36.45
23	**Karun**	64	Aligodarz	49.7	33.4	Talezang	48.76	32.82
22	**Karkheh**	50	Kermanshah and Ravansar	47.15 and 46.65	34.35 and 34.71	Tangsareban	46.84	33.55
13	**Sefidrood**	60	Meyaneh	47.7	37.45	Meyaneh	47.66	37.48
14	**Haraz-Sefidrood**	11	Ramsar and Nowshahr	50.66 and 51.5	36.9 and 36.65	Haratbar	50.83	36.75
15	**Haraz-Ghareso**	15	Gharakhil	52.76	36.45	Ghaem Shahr	52.88	36.29
12	**Talesh-Mordab anzali**	7	Anzali and Rasht	49.46 and 49.6	37.46 and 37.25	Nokhale	49.45	37.33

shows the specification of the basins and their hydrometric and synoptic stations (Fig. 1).

Datasets

This study used the following datasets:

-Observational gauge data

The validation of the data was done using monthly precipitation and runoff datasets sourced from the Iran Meteorological Organization and Iran's Ministry of Energy from 24 selected synoptic and hydrometric stations (for each river basin). The research data were obtained over the 1987–2019 period, which was determined based on the availability of consistent data records with suitable quality and range (Table 1). Observational data were not available for six political basins (red areas in Fig. 1, including Aras,

Attak, West-border, Hamun Hirmand, Hamun Mashkel, and Khaf river basins). Therefore, they were excluded from the research.

-Remotely sensed datasets

Five different datasets on precipitation and runoff from 1987 to 2019 were used here, including:

1) GLDAS-2.1

GLDAS was produced with the cooperation of several institutions. This dataset accurately estimates the weather data by mixing ground-based and satellite measurements of precipitation, humidity, temperature, radiation, wind speed, etc. Moreover, Mosaic, Noah, CLM (Community Land Model), and VIC (Variable Infiltration Capacity) models were used to simulate land-surface states and fluxes (GES

DISC Dataset: GLDAS Catchment Land Surface Model L4 monthly 1.0 × 1.0 degree V2.1 (GLDAS_CLSM10_M 2.1).

2) ERA5

ERA5 is the 5th generation European Centre for Medium-Range Weather Forecasts (ECMWF) atmospheric reanalysis and has greatly surpassed ECMWF Reanalysis Interim (ERA-Interim) in terms of horizontal resolution, spatiotemporal resolution, design simulation, numerical modeling, observational absorption, output frequency, and better model-level display of details (https://cds.climate.copernicus.eu/#!/search?text=ERA5).

3) G-RUN ENSEMBLE (GRUN)

GRUN is a runoff reconstruction based on observation. It employs machine learning algorithms to estimate global runoff (Ghiggi et al. 2019). One of its shortcomings is that it is based on a single atmospheric forcing dataset (GSWP3; (Kim 2017)). Later on, Global RUNoff ENSEMBLE (G-RUN ENSEMBLE), as a new publicly-available global runoff reconstruction, was produced with up to 525 ensemble members through 21 atmospheric forcing datasets (https://figshare.com/articles/dataset/GRUN_Global_Runoff_Reconstruction/9228176).

4) TerraClimate (TERRA)

TerraClimate is a high-spatial-resolution dataset (1/24°, ~ 4 km) of monthly climate and climatic water balance for global terrestrial surfaces. It uses climatically aided interpolation to combine the high-spatial-resolution climatological normal (using the WorldClim dataset) with other coarser resolution and time-varying (i.e., monthly) datasets. This is to generate a monthly dataset of wind speed, precipitation, vapor pressure, solar radiation, and max/min temperature. TerraClimate also creates monthly surface water balance datasets using a water balance model incorporating precipitation, reference evapotranspiration, temperature, and interpolated plant-extractable soil water capacity (https://climate.northwestknowledge.net/TERRACLIMATE).

5) MERRA2

The Modern-Era Retrospective Analysis for Research and Applications, version 2, is a global atmospheric reanalysis generated by the NASA Global Modeling and Assimilation Office. It provides a regularly-gridded (0.5-degree latitude by 5.8-degree longitude) and homogenous record spanning the satellite observing era from 1980 to the present. Compared to MERRA, MERRA2 allows for assimilating modern hyperspectral radiance and microwave observations, along with GPS-Radio Occultation and NASA ozone datasets. It is accessible at https://disc.gsfc.nasa.gov/datasets?project=MERRA-2.

The overall specifications of these products are listed in Table 2. All gridded datasets were re-sampled to 0.5° × 0.5° through the nearest-neighbor interpolation method to match the gridded data from ground observations.

Methodology

The following is an overview of the research methodology (Fig. 2).

As shown in Fig. 2, the research data were sourced from the ERA5, GLDAS, TERRA, MERRA2, and GRUN products. The precipitation and runoff data of mentioned products were validated against observational gauge data. Moreover, fusion-based precipitation and runoff data were assessed to enhance the accuracy of runoff and precipitation evaluations at all river basins. Single and composite indices were calculated using observational data at different time scales for each river basin. For better drought modeling, the AGNES clustering technique as a classification algorithm was employed to cluster ground river basins based on FHMDI into different groups with similar features. Then, for each cluster, four SAI models, namely, GPR, FNN, SVR, and Ensemble were developed under six scenarios to estimate and predict drought using a remotely sensed dataset, and their error indices were determined. In the following, four fusion methods including WB, WMV, EKF, and EW are used for fusing estimations from the four SAI estimator models.

Table 2 Remotely sensed precipitation and runoff products (P, precipitation; R, runoff)

Class	Dataset	Variable	Resolution		Coverage		Ref
			Spatial	Temporal	Spatial	Temporal	
Gauge-based products	GRUN	R	0.5*0.5	1 m	Global	1901–2019	(Ghiggi et al. 2021)
Reanalysis products	ERA5	P&R	0.25*0.25	6 h/1 m	Global	1979–2022	(Hersbach et al. 2020)
	TERRA	P&R	0.04*0.04	1 m	Global	1958–2022	(Abatzoglou et al. 2018)
	GLDAS	P&R	0.25*0.25	3 h/1 m	Global	1948–2022	(Rodell et al. 2004)
	MERRA2	P	0.625*0.5	1 m	Global	1980–2022	(Rienecker et al. 2011)

Fig. 2 The research flowchart
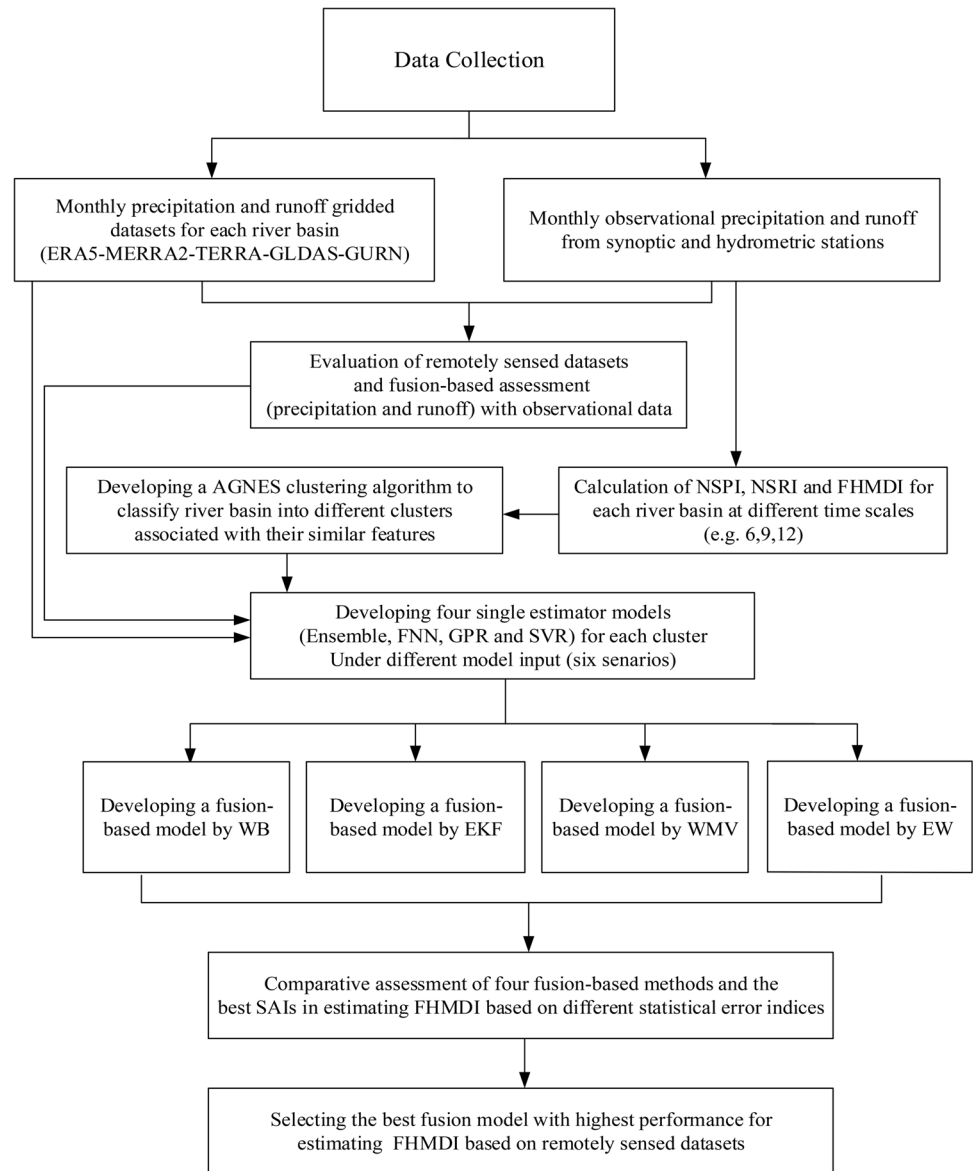
Calculation of runoff based on remotely sensed products

The sum of overland flow, interflow, and groundwater equals runoff in a grid (*q* grid):

$$q_{\text{grid}} = q_{\text{sur}} + q_{g+i} \tag{1}$$

where q_{sur} is the overland flow (m³/s) and $q_{g+\text{inter}}$ is the sum of interflow and groundwater (m³/s). The monthly runoff of various products at gauge sites is the sum of the upstream monthly runoff:

$$q_{\text{gauge}} = \sum q_{\text{grid}} \tag{2}$$

where q_{gauge} is the calculated monthly runoff at gauge sites. This is a popular routing method (Crooks et al. 2014; Wang

et al. 2016) as it is nonparametric (Eq. 2) with no parameter uncertainty.

Three evaluation criteria were used here, namely, modified Kling–Gupta efficiency (KGE), normalized root mean square error (NRMSE), and mean bias error (MBE) because they are commonly utilized in uncertainty evaluations as follows (Knoben et al. 2019):

$$\text{KGE} = 1 - \sqrt[2]{(r-1)^2 + (\beta-1)^2 + (\gamma-1)^2} \tag{3}$$

$$\text{NRMSE} = 100 \times \frac{\sqrt{\frac{\sum_{i=1}^{N}(C_{pi}-C_{ei})^2}{N}}}{C_{e\max} - C_{e\min}} \tag{4}$$

$$\text{MBE} = \frac{\sum_1^N (C_{pi} - C_{ei})}{N} \qquad (5)$$

where N is the sample size, C_e is the observed values, C_p is the calculated value, r is Pearson's linear correlation (measuring the temporal dynamics), γ is the variability ratio (measuring the relative dispersion between simulations and observations), and β is the bias ratio (measuring the total volume) (a value greater than 1 represents an overestimation of the simulations while a value less than 1 represents an underestimation).

Calculation of NSPI, NSRI, and FHMDI indices using ground-based and remotely sensed products

In this research, three drought indices, NSPI, NSRI, and FHMDI, were used for drought analysis. The Standardized Precipitation Index (SPI) is a popular index for assessing meteorological drought. It owes its popularity to its standardized nature, simplicity, and flexibility (Hayes et al. 1999; Sahoo et al. 2015). The Standardized Runoff Index (SRI) was introduced to investigate hydrological drought through the same method used by Mckee et al. (1993), to define SPI, which is the unit standard normal deviation associated with the percentile of hydrologic runoff accumulated over a timescale (Shukla and Wood 2008). Deriving SPI and SRI necessitates fitting a suitable parametric probability distribution function to precipitation data, which may not always be the best distribution function (Angelidis et al. 2012; Guttman 1999). This issue can be resolved using a nonparametric framework to derive NSPI and NSRI and better describe drought.

Regarding the necessity of nonparametric methods in deriving SPIs and SRIs, different statistical tests were used to determine the best probability distribution function for precipitation and runoff data in each ground station. The nonparametric method was employed here considering that different parametric probability distribution functions were fitted to precipitation and runoff data (Alizadeh and Nikoo (2018); Fooladi et al. 2021). Therefore, the probabilities of these data were calculated through the empirical Gringorten plotting position (Farahmand and AghaKouchak 2015):

$$p(x_i) = \frac{i - (44/100)}{n + 12} \qquad (6)$$

where $p(x_i)$ is the empirical probability, i is the rank of non-zero precipitation data, and n represents the sample size. Here, the Standardized Index can be obtained using Eq. 7:

$$\text{SI} = \varphi^\wedge(-1)(p). \qquad (7)$$

where φ is the standard normal distribution function and p is computed empirical probability.

Then, the FHMDI is developed using NSPI, NSRI, and WB fusion-based method s(that will explain at "Fusion-based models") to monitor compound hydrological and meteorological drought for different timescales (6, 9, and 12 months). It should be noted that this new index was calculated on the basis of reanalysis data.

AGglomerative NESting (AGNES) clustering algorithm

Drought can be analyzed and estimated more accurately by using AGNES to classify ground-based observation data into different groups based on similar features. FHMDI (calculated based on observational data) was considered as a clustering criterion to classify the data into various groups based on their feature resemblance. Agglomerative clustering, as a hierarchical clustering algorithm, is an unsupervised machine learning technique dividing the population into clusters with data points being more similar in the same cluster and vice versa (Li et al. 2022).

Single artificial intelligence (SAI) models

Four SAI models, namely, FNN, GPR, Ensemble, and SVR, were employed as estimator models for drought modeling using remotely sensed precipitation and runoff data under six scenarios (as model input) through FHMDI based on river basin's observational data (as output model) that will explain them separately at "Scenarios of simulation." According to AGNES results, the corresponding data for each river basin in different clusters were used to develop SAI models. These SAI models were trained (calibration) and verified (validation) using 80% and 20% of the dataset, respectively. The data were split through shuffled sampling. In addition, different percentage ratios—such as 70:30, 75:25, 80:20, and 85:15—were tested, and the model performance was analyzed in the training and validation stages. Finally, the best output (estimated FHMDI) with the least estimation error was determined for each SAI model based on different statistical error indices. The method for drought estimation and prediction through SAI models is presented in Fig. 3. To enhance accuracy, reliability, and stability of SAIs, different fusion-based models are used to combine them which are presented in the following.

Fusion-based models

Data fusion means aggregation and combination of multi-source data (the individual outputs of different estimation models) to obtain more accurate and reliable solutions as opposed to using single-source data (Dasarathy 1997). Here, four different fusing methods, namely, WB, WMV, EKF, and EW, were used to estimate 6, 9, and 12-month FHMDI using remotely sensed data. Accordingly, the best outputs

Fig. 3 The component of proposed modeling in this study
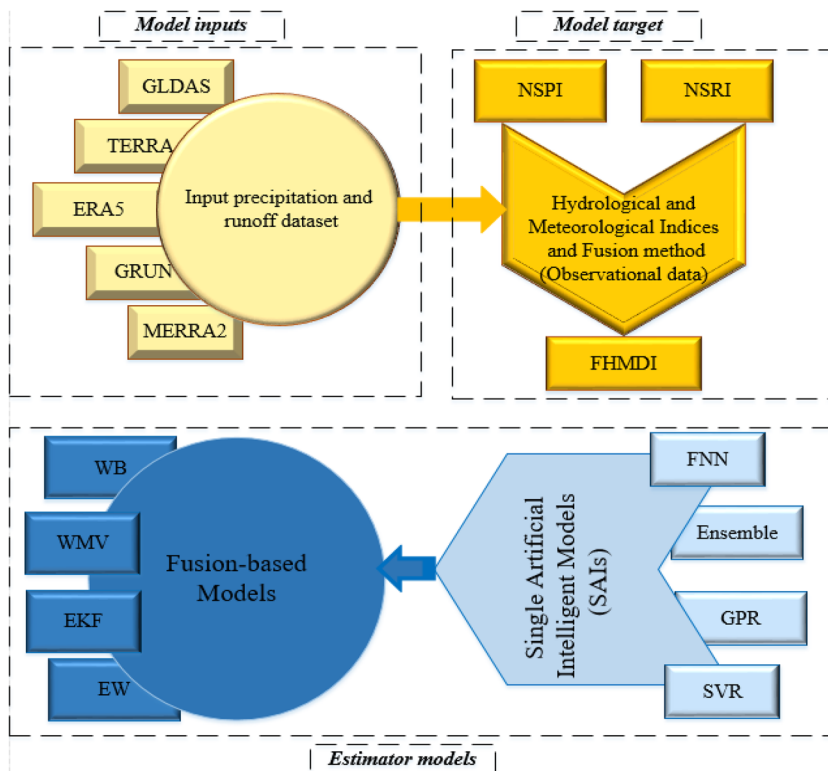
(FHMDI) of the four SAI estimator models (Ensemble, GPR, SVR, and FNN) were fused. A summary of the four methods is given as follows.

a) Wavelet-Based (WB)

Wavelet transform is an important mathematical linear transformation that is used in various fields of science (Xu et al. 2004). The main contribution of this method is to resolve the shortcomings of the Fourier transform. Wavelet transform has a high resolution in both the time domain and the frequency domain. This transformation not only determines the frequency number in the signal but also determines when those frequencies occur in the signal. The wavelet transform enables this by functioning at different scales. In wavelet transform, the signal is first considered with a large scale/window, and its large features are analyzed. In the next step, the signal is examined with small windows, and the small features of the signal are obtained. Suppose there are sensors in a multi-sensor system for observing unknown quantities. Then, the output of the sensor j is:

$$Y_j(t) = Y(t) + n_j(t) \tag{8}$$

where $n_j(t)$ represents the white noise added to the original signal $Y(t)$ in the output $Y_j(t)$. The variance $n_j(t)$ is defined as $\sigma\_j^2 = E[n\_i^2(t)]$, and $E[x]$ is the mathematical expectation of X. If the observations are independent and unbiased, the measure can be estimated using the following LMS estimator:

$$\widehat{Y} = \sum_{j=1}^{N} W_j Y_j \tag{9}$$

where W_j is the weight applied to Y_j and $\sum_{j=1}^{N} W_j = 1$. The estimation variance is also defined as Eq. 10:

$$\sigma^2 = \sum_{j=1}^{N} W_j^2 \sigma_j^2 \tag{10}$$

It represents the jamming noise variance of the j_{th} observation sequence. The observation sequence is referred to as the data sequence obtained from the j_{th} sensor. Hence, σ_j^2 is simply called the variance of the jth observation or sensor sequence.

If the weight of all observation sequences is the same, that is, $W_j = 1/N$. For all j and $\widehat{Y}$ are estimated from Eq. 9, then, the arithmetic mean of observations will be N. The variance of this estimate is calculated by Eq. 11:

$$\sigma_{\text{avg}}^2 = \frac{1}{N^2} \sum_{j=1}^{N} \sigma_j^2 \tag{11}$$

Although the arithmetic mean is widely used for estimating measurements from multiple independent observations, the estimates are not optimal regarding the least mean squared error. Therefore, to minimize the

polynomial in Eq. 10, the optimal weights should be equal to 1 ($\sum_{j=1}^{N} W_j = 1$) which can be calculated through Eq. 12:

$$W_j = \frac{1}{\sigma_j^2 \sum_{j=1}^{N} \frac{1}{\sigma_j^2}} \qquad (12)$$

Therefore, the minimum variance estimated from Y will be calculated as Eq. 13:

$$\sigma_{\min}^2 = \frac{1}{\sum_{j=1}^{N} \frac{1}{\sigma_j^2}}. \qquad (13)$$

In this case, the estimator is consistent and unbiased. It can also be proven that $\sigma_{\min}^2$ is not only smaller than the variance of any observed sequence but also smaller than Eq. 11. If it is possible to obtain $\sigma_{\min}^2 = \frac{1}{\sum_{j=1}^{N} \frac{1}{\sigma_j^2}}$ in advance, relations 9 and 12 can be used to obtain the optimal estimation of the measurement in terms of the minimum mean squared error.

b) Weighted Majority Voting (WMV)

Majority voting is a simple and highly effective linear hybrid group learning method. For example, in real-world research on a particular issue, in case some experts are more competent than others, weighting the decisions of those qualified experts may improve the overall performance more so than mere multi-voting (Ekbal and Saha 2012, 2011). The same problem exists in combining results when using SAI algorithms because finding the best weight is important. If the weight coefficients are not chosen correctly, it will yield poor results. Now, to combine the dataset, the weight combination is used according to Eq. 14, which is derived from the single-layer perceptron neural network (de Almeida et al. 2020).

$$W_O = \left(H^T.H + \lambda.I\right)^{-1}.H^T.T \qquad (14)$$

where H is the input data, T is the target vector, λ is a small fixed value, and I is the singular matrix, which is also known as the penalty because it penalizes large weights in the optimization process. Now, having the optimal weights, by multiplying it with the data, a combined and optimal target vector can be obtained through Eq. 15.

$$T = H * WO \qquad (15)$$

c) Extended Kalman Filter (EKF)

The EKF algorithm is used to merge the input data (taken from different datasets). This algorithm is applied in two phases (Kaczmarek et al. 2022). Suppose all system information is available up to sample $k-1$. Then, based on the system's mathematical model and the available data up to time $k-1$, an initial estimate of the state variables in sample k is calculated. We call this step of the Kalman filter the prediction process. Now, naturally, a new measurement is made by the sensors at time k, that is, y_k becomes available. In the second step of the Kalman filter, which is called the update phase, the prediction made in the first step is improved using the newly available data in order to obtain the final estimated states in the K sample. The prediction phase is performed through the following two equations:

$$\widehat{x}_{k|k-1} = f(\widehat{x}_{k-1}, u_{k-1}) \qquad (16)$$

$$P_{k|k-1} = (F_{k-1} P_{k-1} F_{k-1}^T) + Q_{k-1} \qquad (17)$$

In these relations, $\widehat{x}_{k-1}$ is the vector of estimated states in the sample $k-1$; u_{k-1} is the control vector in sample $k-1$; Q_{k-1} is the noise matrix in sample $k-1$; P_{k-1} is the covariance matrix in the sample $k-1$; $\widehat{x}_{k|k-1}$ is the prediction of the state variable in sample k based on the information from the system up to the sample $k-1$; $P_{k|k-1}$ is the prediction of the covariance matrix in sample k based on information from the system up to the sample $k-1$; finally, F_k and F_{k-1}^T are the linearized dynamics obtained through Taylor linearization and the T mark on it indicates that it is a transpose.

$$F_k = \text{frac } \partial_f \partial_x|_{xk-1}, \qquad (18)$$

The update phase of the EKF is performed as follows:

$$K_k = P_{k|k-1} H^T (H_k P_{k|k-1} H^T + R_k)^{-1}, \qquad (19)$$

$$\widehat{x}_k = \widehat{x}_{k|k-1} + K_k \left[z_k - h(\widehat{x}_{k|k-1})\right], \qquad (20)$$

$$P_k = \left(1 - K_k H_k\right) P_{k|k-1}, \qquad (21)$$

Here, H_k is the measured linearized dynamics, which is used in the update phase. This matrix is also calculated as follows.

$$H_k = \text{frac} \partial_h \partial_x|_{\widehat{x}_{k|k-1}} \qquad (22)$$

In the formula, z_k is the output measured by the sensors. Therefore, in the first step, the Kalman interest (K_k) is calculated and then the final estimate of the state variables ($\widehat{x}_k$) and the covariance matrix (P_k) in the sample k are calculated. Phrase $\left[z_k - h(\widehat{x}_{k|k-1})\right]$ also indicates the difference between the actual output measured by the sensors and the output obtained in the prediction phase.

d) Entropy Weight (EW)

EW is a linear method that helps to weigh indicators (Zhu et al. 2018). In this method, the indicator-derived matrix is first standardized and the entropy of every indicator is calculated:

$$H_j = \frac{-\sum_{i=1}^{m} f_{i,j} * \ln(f_{i,j})}{\text{Ln}(m)} \tag{23}$$

In which

$$f_{ij} = \frac{\text{abs}(r_{i,j})}{\sum_{i=1}^{m} \text{abs}(r_{i,j})} \tag{24}$$

where f_{ij} is the value of the index matrix, j is the variable, m is the year, and i is the month. The indicator weight is calculated using Eqs. 25 and 26:

$$D_j = 1 - H_j \tag{25}$$

$$w_j = \frac{D_j}{\sum_{j=1}^{n} D_j} \tag{26}$$

where w_j is the assigned weight of each variable, which should be equal to 1 ($\sum_{j=1}^{n} w_j = 1$); D_j represents a measure of the entropy for the jth variable.

Scenarios of simulation

To make input model, six scenarios are considered as follows:

- S1 (MI-8 V): Model input including four datasets of precipitation (TEERA, MEERA2, GLDAS, and ERA5) and four datasets of runoff (TEERA, MEERA2, GLDAS, and ERA5)
- S2 (MI-2 V-F1): Two variables as representative of precipitation and runoff with datasets of each variable combined by WB fusion method
- S3 (MI-2 V-F2): Two variables as representative of precipitation and runoff with datasets of each variable combined by WMV fusion method
- S4 (MI-2 V-F3): Two variables as representative of precipitation and runoff with datasets of each variable combined by EKF fusion method
- S5 (MI-2 V-F4): Two variables as representative of precipitation and runoff with datasets of each variable combined by EW fusion method
- S6 (MI-2 V): Two variables as representative of precipitation and runoff selected based on the results of single- and multi-product models versus local observations)

Results

Temporal and spatial assessment of monthly runoff and precipitation gridded products at the river basins

First, the upstream basin of the selected hydrometric station was determined at each river basin. Then, upstream runoff for each product was measured against observational monthly point-based data from the selected stations. The result of the evaluation criteria for runoff at the monthly scale can be observed for all river basins in Fig. 4. As it is clear, all of the products showed that there is a higher correlation coefficient (KGE between 0 and 1) in winter (Jan-Feb-Mar) (40%) and spring (Apr-May-Jun) (30%) than in other seasons (Fig. 4a). GRUN and ERA5 products had the highest correlation (50%, 42%, 40%, and 30% above 0.5, respectively) than other products. It should be noted that all negative KGE values are related to high bias ratio values. The NRMSE was the lowest for GRUN year-round (with an average value of 33%) (Fig. 4b). GRUN had the highest accuracy (lower than 1) in the Mand, Gavkhuni, Gharesu Gorgan, Karun, Karkheh, Haraz-Ghareso, and Talesh-Mordab Anzali river basins, with the average NRMSE being the lowest in Karkheh (0.7) and the highest in Mand (0.99) river basins. All of the products had the lowest error in Karun and Gavkhuni river basins and the highest error in the Central Desert (even GRUN product). According to MBE values, GLDAS overestimated runoff in all of the seasons (80% mean values), whereas GRUN, ERA5, and TERRA underestimated runoff compared to observational values (with average values of 52%, 55%, and 62%, respectively) (Fig. 4c) among all river basins. All products mostly overestimated runoff during four seasons in the Siahkooh, Central Desert, Ghareghoom, Namke Lake, Tasht Bakhtegan, and Haraz-Sefidrood river basins, but not in Helle, Hamun Jazmurian, Karun, and Gavkhuni river basins.

Figure S1 (Supplementary Material) shows the result of the evaluation criteria for precipitation at the monthly scale for all river basins. As can be observed, all of the products showed a higher correlation coefficient (KGE between 0 and 1) in winter (Jan-Feb-Mar) (80%) and spring (Apr-May-Jun) (82%) than in other seasons (Figure S1-a). All products had a KGE value higher than 0.5 in 70% of the cases. NRMSE was the lowest and highest for MERRA2 and ERA5 products during four seasons (with an average value of 60% and 30%, respectively) (Figure S1-b). MERRA2 had the highest accuracy (lower than 1) in Haraz-Ghareso, Haraz-Sefidrood, and Gharesu-Gorgan (with an average value of 65%). According to MBE values, GLDAS over- and under-estimates precipitation

Fig. 4 The results of evaluation criteria for runoff datasets with observed runoff in different months and river basins (ER: ERA5; GR: GRUN; GL: GLDAS; TE: TERRA) (1987–2019)
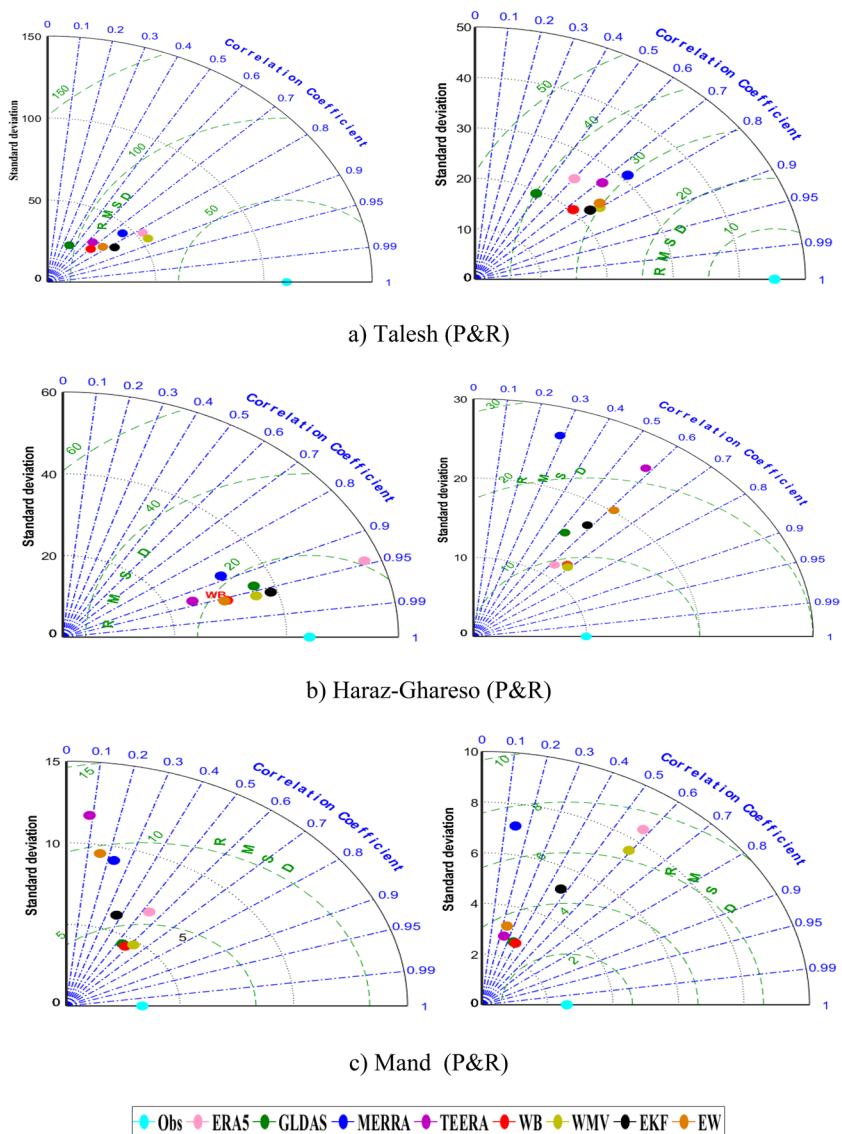

a) KGE

b) NRMSE

c) MBE
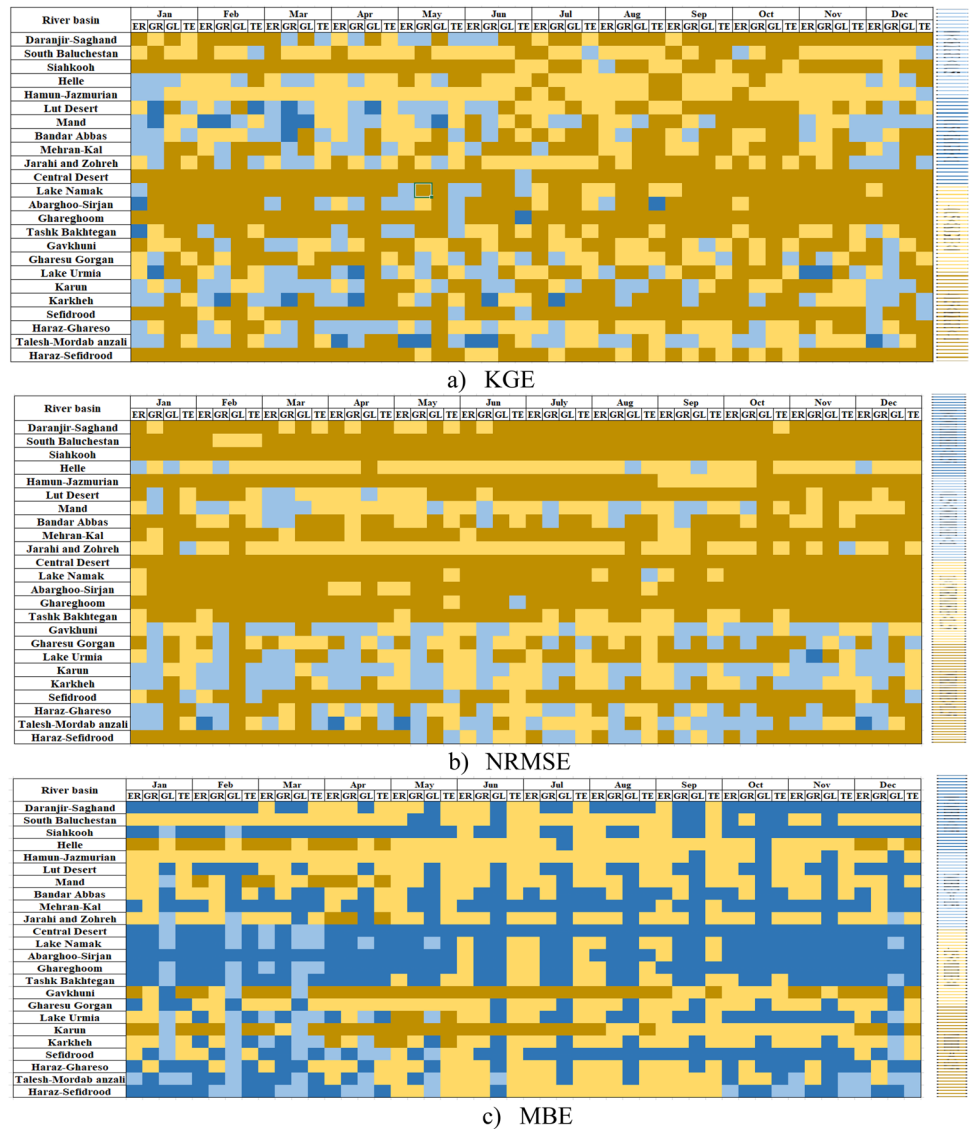
in all of the seasons and river basins (50% mean values), while MERRA2, ERA5, and TERRA under-estimate precipitation compared to observational values (with average values of 72%, 77%, and 64%, respectively) (Figure S1-c).

Fusion-based assessment of runoff and precipitation gridded products at the river basins

Considering the various climate zones across Iran, the precipitation and runoff datasets do not have the same accuracy for different river basins, which makes it difficult to choose the best product for a specific area. The fusion-based approaches can be used to overcome this issue by increasing the accuracy of remotely sensed datasets. In this section, the combined remotely sensed products were investigated using four fusion-based methods. The Taylor diagrams in

Fig. 5 demonstrate the data accuracy in each dataset and model compared against local observations at some river basins as an example. As can be seen, WMV had the closest performance to local observation in the Talesh river basin (Fig. 5a). WMV and WB methods had a good performance for precipitation and runoff, respectively, in Haraz-Ghareso. WMV showed the highest accuracy (~60%) compared to single-source precipitation and runoff products. In addition, WMV (50%) and EKF (20%) outperformed WB and EW methods in merging data in all river basins. Figure S2 provides information on some statistical metrics, including KGE, NRMSE, and MBE obtained from each precipitation and runoff product and four fusion-based models. It can be seen that all products and fusion-based models yielded different outputs compared to local observations. For instance, EKF fusion-based model outperformed other methods (with the lowest NRMSE 0.7 and highest KGE 0.83) for

Fig. 5 Taylor diagrams of precipitation data on remotely sensed datasets and two fusion-based models compared to local observations in the 1987–2019 period (left: precipitation, right: runoff)

a) Talesh (P&R)

b) Haraz-Ghareso (P&R)

c) Mand (P&R)

Obs · ERA5 · GLDAS · MERRA · TEERA · WB · WMV · EKF · EW

both precipitation and runoff in Helle, while MERRA2 and GRUN products had a good performance for precipitation and runoff, respectively, in the Lut Desert river basin. This difference may be due to the poor performance of products, which were not improved after fusion.

Fusion-based Hydro-Meteorological Drought Index (FHMDI)

Individual indices including hydrological and meteorological drought indices were computed for the selected stations and different time scales (e.g., 6, 9, and 12 months). NSRI and NSPI appear to be good solutions for the problem of probability distribution fitting, because a fixed distribution may not always be the best choice. According to Table 3, the best probability distribution functions were used for precipitation and runoff data of each ground station

through the Kolmogorov–Smirnov test. Results showed no relevance between the datasets and the probability distribution functions. Hence, NSPI and NSRI were used as nonparametric meteorological and hydrological drought indices in the river basins of Iran. Then, a composite drought index, called FHMDI, was calculated to monitor compound hydrological and meteorological drought using WB method.

Compound drought modeling based on SAI models

Here, 24 river basins were classified into different clusters aiming to attain better composite drought prediction and estimation results. The AGNES model provided four clusters based on their feature similarity (FHMDI) (Table 4). Figure 6 shows the value of FHMDI12 in all clusters (for all river basins) as an example. FHMDI12 variation in monthly

Table 3 Top probability distribution functions for precipitation and runoff data of selected synoptic and hydrometric station

Synoptic station	Distribution function	Statistical test (KS)	Hydrometric station	Distribution function	Statistical test (KS)
Miyane	Gen.Gamma	0.09	**Miyane Shrichay**	Johnson SB	0.14
Takab	Gen.Extreme value	0.1	**Safakhane**	Dagum	0.05
Gharakhil	Wakeby	0.02	**Shirgah Talar**	Pearson6	0.02
Gorgan	Wakeby	0.02	**Gorgan**	Log normal	0.03
Kermanshah	Gen.Extreme value	0.16	**Tangsareban**	Log normal(3p)	0.03
Omidieh	Power function	0.16	**Gargar**	Log normal	0.02
Koohrang	Gen.Extreme value	0.16	**Ghale shahrokh**	Log-Logistic	0.05
Mashhad	Gen.Extreme value	0.13	**Moshang**	Log-Logistic	0.07
Shiraz	Wakeby	0.21	**Band Bahman**	Burr	0.06
Sirjan	Wakeby	0.21	**Jamjaz&Soj**	Log-Logistic	0.09
Kashan	Gen.Extreme value	0.17	**Pol Hanjen**	Johnson SB	0.07
Torbat Heydareh	Gen.Extreme value	0.16	**Hosein Abad Jangal**	Wakeby	0.3
Anzali	Johnson SB	0.02	**Nokhale**	Wakeby	0.03
Ramsar	Wakeby	0.02	**Harat bar**	Johnson SB	0.06
Ghom	Gen.Extreme value	0.15	**Jalayer**	Burr	0.05
Aligodarz	Wakeby	0.15	**Talezang**	Johnson SB	0.02
Kerman	Wakeby	0.21	**Godarz&Jirofto**	Log normal(3p)	0.02
Iranshahr	Power function	0.13	**Daman**	Burr	0.03
Chabahar	Normal	0.35	**Kahir**	Beta	0.17
Minab	Beta	0.28	**Berentin Minab**	Wakeby	0.07
Bandarlenge	Power function	0.29	**Dezhgan**	Burr	0.04
Dogonbadan	Gen.Logistic	0.2	**Chiti Borki**	Johnson SB	0.03
Bam	Power function	0.1	**Sorakh Mar**	Gen.Extreme value	0.14
Abadeh	Power function	0.18	**Tangbolagh**	Wakeby	0.11

Table 4 Results of AGNES algorithm for river basin classification

| Clusters based on AGNES algorithm	River basin number
Cluster 1	29, 42
Cluster 2	24, 25, 26, 27, 28, 43, 44, 46, 47, 48, 49, 60
Cluster 3	13, 22, 23, 30, 41, 42
Cluster 4	12, 14, 15, 16

time series from 1987 to 2019 in all river basins shows that the highest drought severity (less than -2) and extent (100% of region or all pixel) occurred in the 1999–2000 period (24 months) in all clusters across Iran.

Table 5 demonstrates the statistical error metrics for SAI models in FHMDI predictions at a 12-month timescale for different clusters in the calibration and validation stages, as an example. It can be seen that the error index differences at the validation stage are negligible for the four models in clusters 1, 3, and 4, suggesting that they are suitably trained and verified. Although none of

the models is entirely superior to the others, GPR slightly outperformed other models under scenario 1 (MI-8 V) with the highest KGE (0.94) and lowest NRMSE (0.06). In cluster 2, the ensemble model with the average values of KGE $= 0.95$ and NRMSE $= 0.07$ had the lowest estimation error under scenario 1 (MI-8 V). Generally, drought modeling was satisfactory under scenario 1 in all clusters, while it was better in clusters 1 and 2 than in clusters 3 and 4.

Based on the results, scenario 2 (MI-2 V and WB method) also had a good performance (after scenario 1) in clusters 1 and 2 (KGE $= 0.87$ and NRMSE $= 0.09$), while there was no other satisfactory scenario in clusters 3 and 4. In other words, other scenarios performed poorly in clusters 3 and 4. Moreover, the results of the four SAI models at different time scales showed that the model performance improved by increasing the time scale (Table S1 and Table S2; respectively, 6- and 9-month timescales). The scatter plots of the estimated and observed 12-month FHMDI under scenario 1 are presented in Fig. 7. As can be seen, Ensemble and GPR models had a better correlation than other models in all clusters.

Fig. 6 The change in the monthly FHMDI 12 in all clusters (for each river basin) in monthly time series from 1987 to 2019
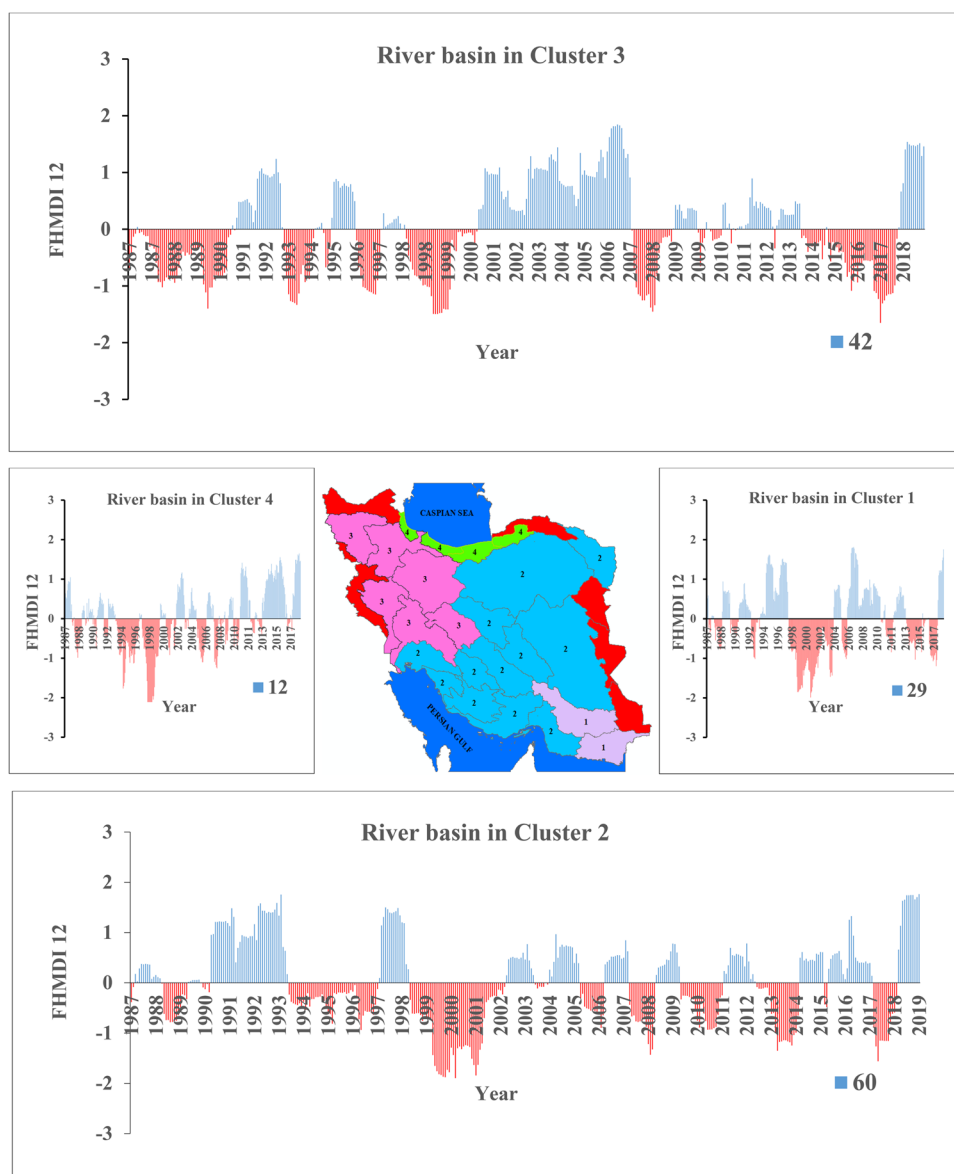
Compound drought modeling based on fusion-based methods

Four fusion-based methods including WB, EKF, WMV, and EW were used for improving the SAI results under scenario 1 (since drought modeling had the best performance under this scenario). Table 6 presents the results of fusion-based methods in predicting FHMDI at the 12-month time scale for the calibration and validation stages in four clusters. WMV had the lowest error for all clusters. WMV also had the best results in cluster 3 with NRMSE of 0.02 and KGE of 0.99. Based on the NRMSE indicator, WMV enhanced the precision of the predicted FHMDI by 48%, 60%, 56%, and 45% compared to the best SAI model for clusters 1, 2, 3, and 4, respectively. Tables S5 and S6 show that fusion methods performed

poorly in the short-term (6) compared to the long-term (12) timescale.

Figure 8 demonstrates the predicated FHMDI at a 12-month time scale using WMV for four ground stations in four clusters. As can be seen, WMV with $R^2 = 0.99$ had the best performance in cluster 3. Figure 9 shows that FHMDI estimations in the Hamun river basin (as an example) performed better in the 12-month ($R^2 = 0.9783$) than in the 6-month ($R^2 = 0.8033$) timescale.

Discussion

Precise prediction of precipitation and runoff is a significant challenge in the study of drought characterization and monitoring (Nassaj et al. 2022). Additionally, drought modeling

Table 5 The evaluation criteria for SAI models in estimating 12-month FHMDI for calibration and validation stages in all clusters under different scenarios

Cluster	Scenario	Model input	SAI models	Calibration			Validation		
				KGE	NRMSE	MBE	KGE	NRMSE	MBE
1	**S1**	MI-8 V: P (TE, ME, GL, and ER) and R (TE, GL, and ER.GR)	Ensemble	0.92	0.04	0.11	0.93	0.06	0.17
			SVR	0.76	0.11	0.35	0.87	0.10	0.29
			FNN	0.91	0.07	0.24	0.91	0.08	0.24
			GPR	0.99	0.01	0.03	0.94	0.06	0.12
	S2	MI-2 V-F1: PFB1 (TE, ME, GL, and ER) and RFB1 (TE, GL, and ER.GR)	Ensemble	0.86	0.07	0.20	0.88	0.09	0.29
			SVR	0.68	0.12	0.39	0.83	0.10	0.36
			FNN	0.77	0.11	0.37	0.88	0.09	0.37
			GPR	0.78	0.11	0.28	0.89	0.09	0.30
	S3	MI-2 V-F2: PFB2 (TE, ME, GL, and ER) and RFB2 (TE, GL, and ER.GR)	Ensemble	0.82	0.08	0.23	0.82	0.09	0.26
			SVR	0.46	0.16	0.45	0.68	0.12	0.41
			FNN	0.49	0.15	0.45	0.68	0.13	0.47
			GPR	0.76	0.10	0.31	0.83	0.09	0.29
	S4	MI-2 V-F3: PFB3 (TE, ME, GL, and ER) and RFB3 (TE, GL, and ER.GR)	Ensemble	0.85	0.07	0.20	0.85	0.09	0.28
			SVR	0.70	0.13	0.39	0.81	0.10	0.39
			FNN	0.73	0.12	0.35	0.83	0.11	0.35
			GPR	0.83	0.09	0.27	0.84	0.10	0.27
	S5	MI-2 V-F4: PFB3 (TE, ME, GL, and ER) and RFB3 (TE, GL, and ER.GR)	Ensemble	0.86	0.07	0.16	0.74	0.11	0.35
			SVR	0.71	0.12	0.13	0.81	0.12	0.17
			FNN	0.76	0.12	0.28	0.83	0.11	0.53
			GPR	0.82	0.10	0.86	0.70	0.13	0.13
	S6	MI-2 V-selected variables (P:WMV and R:EKF)	Ensemble	0.84	0.07	0.16	0.86	0.09	0.33
			SVR	0.71	0.12	0.18	0.76	0.12	0.36
			FNN	0.77	0.11	0.61	0.83	0.11	0.59
			GPR	0.80	0.10	0.45	0.84	0.10	0.11
2	**S1**	MI-8 V: P (TE, ME, GL, and ER) and R (TE, GL, and ER.GR)	Ensemble	0.94	0.04	0.11	0.95	0.07	0.18
			SVR	0.82	0.10	0.32	0.90	0.10	0.30
			FNN	0.91	0.08	0.27	0.91	0.10	0.26
			GPR	0.99	0.01	0.03	0.88	0.08	0.20
	S2	MI-2 V-F1: PFB1 (TE, ME, GL, and ER) and RFB1 (TE, GL, and ER.GR)	Ensemble	0.88	0.07	0.24	0.88	0.09	0.26
			SVR	0.74	0.12	0.41	0.84	0.11	0.35
			FNN	0.83	0.10	0.41	0.89	0.10	0.37
			GPR	0.82	0.10	0.36	0.87	0.10	0.31
	S3	MI-2 V-F2: PFB2 (TE, ME, GL, and ER) and RFB2 (TE, GL, and ER.GR)	Ensemble	0.85	0.08	0.23	0.89	0.10	0.34
			SVR	0.67	0.15	0.45	0.81	0.16	0.47
			FNN	0.72	0.13	0.37	0.83	0.13	0.39
			GPR	0.80	0.11	0.40	0.77	0.14	0.41
	S4	MI-2 V-F3: PFB3 (TE, ME, GL, and ER) and RFB3 (TE, GL, and ER.GR)	Ensemble	0.87	0.07	0.23	0.89	0.10	0.34
			SVR	0.76	0.12	0.40	0.87	0.12	0.37
			FNN	0.81	0.11	0.40	0.86	0.12	0.36
			GPR	0.80	0.11	0.37	0.87	0.12	0.36
	S5	MI-2 V-F4: PFB3 (TE, ME, GL, and ER) and RFB3 (TE, GL, and ER.GR)	Ensemble	0.88	0.07	0.16	0.88	0.10	-0.12
			SVR	0.77	0.13	0.18	0.85	0.11	0.12
			FNN	0.80	0.12	0.67	0.84	0.11	0.16
			GPR	0.81	0.11	0.45	0.85	0.11	0.19
	S6	MI-2 V-selected variables (P:TERRA and R:GRUN)	Ensemble	0.81	0.09	0.54	0.88	0.09	-0.15
			SVR	0.67	0.14	0.17	0.78	0.14	-0.17
			FNN	0.74	0.13	0.45	0.88	0.12	0.25
			GPR	0.71	0.13	0.37	0.85	0.13	0.27

Table 5 (continued)

Cluster	Scenario	Model input	SAI models	Calibration			Validation		
				KGE	NRMSE	MBE	KGE	NRMSE	MBE
3	**S1**	MI-8 V:	Ensemble	0.90	0.05	0.16	0.90	0.07	0.17
		P (TE, ME, GL, and ER) and R (TE, GL, and ER.GR)	SVR	0.73	0.13	0.05	0.85	0.11	0.26
			FNN	0.95	0.06	0.15	0.91	0.07	0.19
			GPR	0.99	0.01	0.06	0.94	0.05	0.11
	S2	MI-2 V-F1:	Ensemble	0.83	0.08	0.01	0.78	0.11	0.26
		PFB1 (TE, ME, GL, and ER) and RFB1 (TE, GL, and ER.GR)	SVR	0.63	0.16	0.11	0.76	0.15	0.36
			FNN	0.70	0.14	0.21	0.76	0.15	0.37
			GPR	0.85	0.08	0.18	0.80	0.12	0.29
	S3	MI-2 V-F2:	Ensemble	0.81	0.09	0.11	0.82	0.12	0.22
		PFB2 (TE, ME, GL, and ER) and RFB2 (TE, GL, and ER.GR)	SVR	0.65	0.15	0.10	0.77	0.14	-0.11
			FNN	0.73	0.13	0.19	0.79	0.13	-0.11
			GPR	0.75	0.12	0.18	0.79	0.13	-0.12
	S4	MI-2 V-F3:	Ensemble	0.76	0.10	0.07	0.60	0.21	0.12
		PFB3 (TE, ME, GL, and ER) and RFB3 (TE, GL, and ER.GR)	SVR	0.36	0.19	0.12	0.53	0.22	0.16
			FNN	0.55	0.16	0.22	0.57	0.23	0.16
			GPR	0.84	0.07	0.15	0.49	0.23	0.15
	S5	MI-2 V-F4:	Ensemble	0.75	0.10	0.14	0.79	0.10	0.48
		PFB3 (TE, ME, GL, and ER) and RFB3 (TE, GL, and ER.GR)	SVR	0.43	0.18	0.16	0.60	0.15	0.58
			FNN	0.56	0.16	0.15	0.72	0.13	0.45
			GPR	0.75	0.11	0.66	0.82	0.11	0.29
	S6	MI-2 V-selected variables (P:WMV and R:EKF)	Ensemble	0.82	0.08	0.10	0.85	0.11	0.21
			SVR	0.46	0.18	0.19	0.43	0.17	0.20
			FNN	0.66	0.14	0.38	0.60	0.15	0.11
			GPR	0.74	0.12	0.26	0.79	0.12	0.12
4	**S1**	MI-8 V:	Ensemble	0.89	0.04	0.06	0.84	0.08	0.20
		P (TE, ME, GL, and ER) and R (TE, GL, and ER.GR)	SVR	0.74	0.12	0.18	0.84	0.12	0.34
			FNN	0.88	0.08	0.05	0.87	0.11	0.21
			GPR	0.98	0.02	0.03	0.95	0.06	0.15
	S2	MI-2 V-F1:	Ensemble	0.70	0.10	0.17	0.63	0.17	0.41
		PFB1 (TE, ME, GL, and ER) and RFB1 (TE, GL, and ER.GR)	SVR	0.50	0.16	0.33	0.66	0.18	0.50
			FNN	0.53	0.15	0.24	0.65	0.16	0.49
			GPR	0.54	0.15	0.30	0.60	0.17	0.42
	S3	MI-2 V-F2:	Ensemble	0.69	0.10	0.12	0.64	0.13	0.38
		PFB2 (TE, ME, GL, and ER) and RFB2 (TE, GL, and ER.GR)	SVR	0.37	0.17	0.22	0.60	0.19	0.45
			FNN	0.56	0.15	0.20	0.65	0.14	0.41
			GPR	0.61	0.13	0.17	0.63	0.14	0.41
	S4	MI-2 V-F3:	Ensemble	0.68	0.11	0.15	0.66	0.16	0.49
		PFB3 (TE, ME, GL, and ER) and RFB3 (TE, GL, and ER.GR)	SVR	0.41	0.17	0.33	0.57	0.18	0.48
			FNN	0.57	0.15	0.24	0.68	0.16	0.44
			GPR	0.60	0.13	0.28	0.66	0.16	0.47
	S5	MI-2 V-F4:	Ensemble	0.71	0.10	0.17	0.49	0.19	-0.20
		PFB3 (TE, ME, GL, and ER) and RFB3 (TE, GL, and ER.GR)	SVR	0.26	0.18	0.36	0.52	0.18	-0.20
			FNN	0.49	0.15	0.35	0.48	0.19	-0.21
			GPR	0.68	0.12	0.18	0.59	0.19	-0.16
	S6	MI-2 V-selected variables (P:TERRA and R:GRUN)	Ensemble	0.65	0.11	0.10	0.68	0.14	0.67
			SVR	0.30	0.18	0.14	0.36	0.19	0.46
			FNN	0.35	0.17	0.20	0.44	0.17	0.11
			GPR	0.45	0.16	0.15	0.54	0.16	0.19

Fig. 7 The performance of SAI models in estimating 12-month FHMDI in different clusters (cluster 1: South Baluchestan, cluster 2: Mehran-Kal, cluster 3: Lake Namak, and cluster 4: Haraz-Ghareso river basins) for all data (1987–2019) under scenario 1
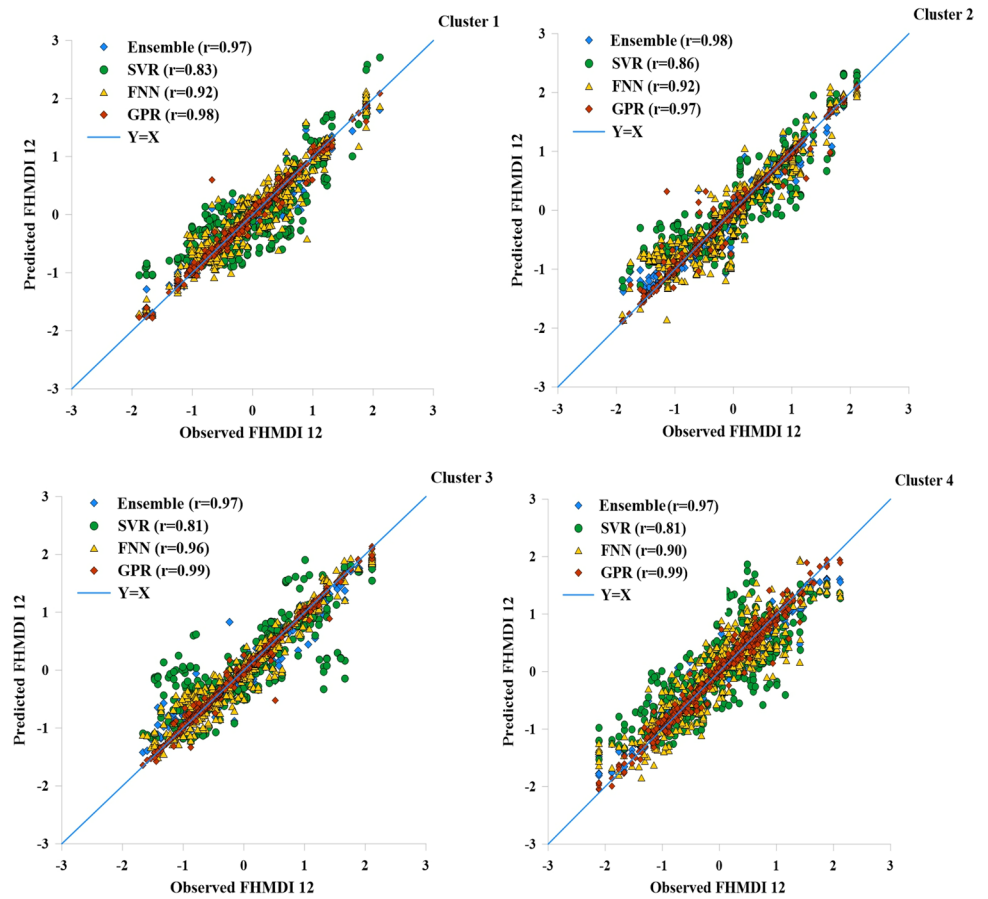

Table 6 The evaluation criteria for four fusion models in estimating 12-month FHMDI for calibration and validation stages under scenario 1

Time scale	Cluster	Fusion models	Calibration			Validation		
			KGE	NRMSE	MBE	KGE	NRMSE	MBE
12	**1**	**Wavelet-Based**	0.87	0.04	0.11	0.86	0.05	0.14
		Weighted Majority Voting	0.99	0.02	0.05	0.97	0.03	0.03
		Extended Kalman Filter	0.96	0.04	0.12	0.89	0.05	0.15
		Entropy Weight	0.91	0.01	0.07	0.84	0.07	0.16
	2	**Wavelet-Based**	0.92	0.05	0.14	0.91	0.06	0.13
		Weighted Majority Voting	0.98	0.04	0.08	0.97	0.04	0.07
		Extended Kalman Filter	0.95	0.05	0.11	0.93	0.06	0.09
		Entropy Weight	0.91	0.05	0.17	0.84	0.09	0.18
	3	**Wavelet-Based**	0.92	0.04	0.10	0.90	0.05	0.12
		Weighted Majority Voting	0.97	0.02	0.05	0.95	0.02	0.05
		Extended Kalman Filter	0.94	0.04	0.10	0.91	0.04	0.11
		Entropy Weight	0.90	0.07	0.11	0.88	0.08	0.12
	4	**Wavelet-Based**	0.94	0.05	0.13	0.91	0.04	0.12
		Weighted Majority Voting	0.97	0.03	0.10	0.96	0.03	0.10
		Extended Kalman Filter	0.93	0.05	0.14	0.90	0.04	0.12
		Entropy Weight	0.92	0.07	0.17	0.90	0.06	0.14

is essential for mitigating its impacts, informing the public about its consequences, and planning water resources (Docheshmeh Gorgij et al. 2022).

Several studies have evaluated the performance of different gridded precipitation datasets over Iran, unlike runoff. Among these studies, one conducted by Saemian

Fig. 8 Predicted 12-month FHMDI using remotely sensed datasets based on WMV in four river basins from different clusters for all data (1987–2019)
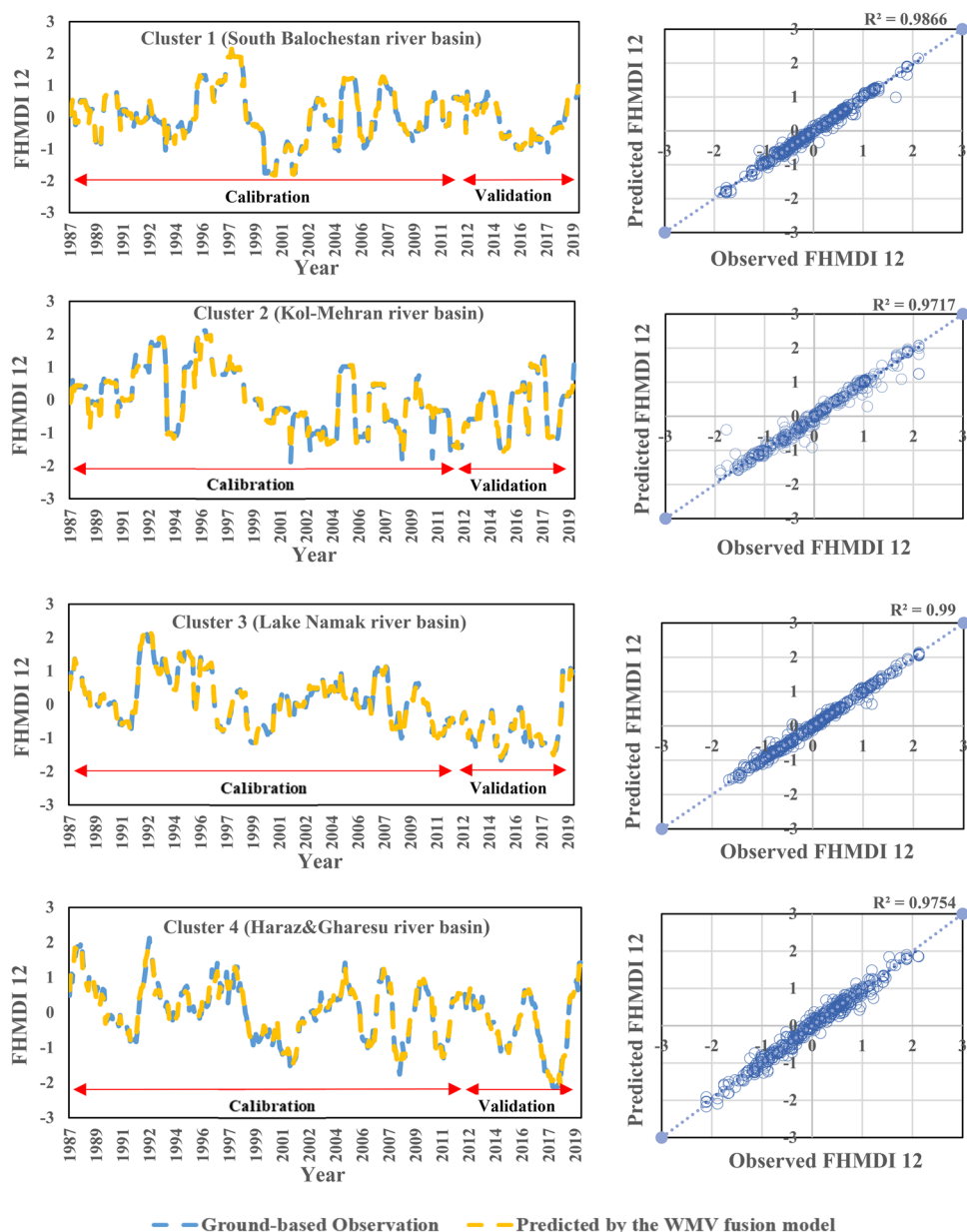
et al. ([2021]) demonstrated the high accuracy of MERRA2 over Iran, which aligns with the findings of this research. Similar conclusions have been reported by other studies regarding the accuracy of MERRA2 in various regions worldwide such as Chen et al. ([2019]), Kuswanto and Naufal ([2019]), Le et al. ([2020]), Odon et al. ([2019]), and Ullah et al. ([2021]).

Our findings regarding the combination of multiple precipitation datasets align with the results reported by Beck et al. ([2017]), Xu et al. ([2020]), and Fooladi et al. ([2023]). These studies also demonstrated that combining multiple precipitation datasets resulted in higher accuracy compared to relying on a single dataset alone. It is important to note that there is currently no existing study specifically focused on the combination of runoff datasets for Iran or any other region. Therefore, our research on the assessment of runoff, particularly in Iran, represents a novel contribution to the field.

The performance of FHMDI at all river basins was also measured against numerous drought events in Iran during 1998–2001(Morid et al. [2006]; Hosseini et al. [2023]) which confirmed their efficiency (composite drought index) in drought monitoring (as can be observed at the next section).

Previous studies such as Mishra and Desai ([2006]), Morid et al. ([2007]), Bacanli et al. ([2009]), and Marj and Meijerink ([2011]) have provided evidence supporting the effectiveness of machine learning models in accurately forecasting drought. These studies highlight the potential of machine learning

Fig. 9 Predicted 6, 9, and 12-month FHMDI using remotely sensed datasets based on WMV in Karun river basin from different clusters for all data (1987–2019)
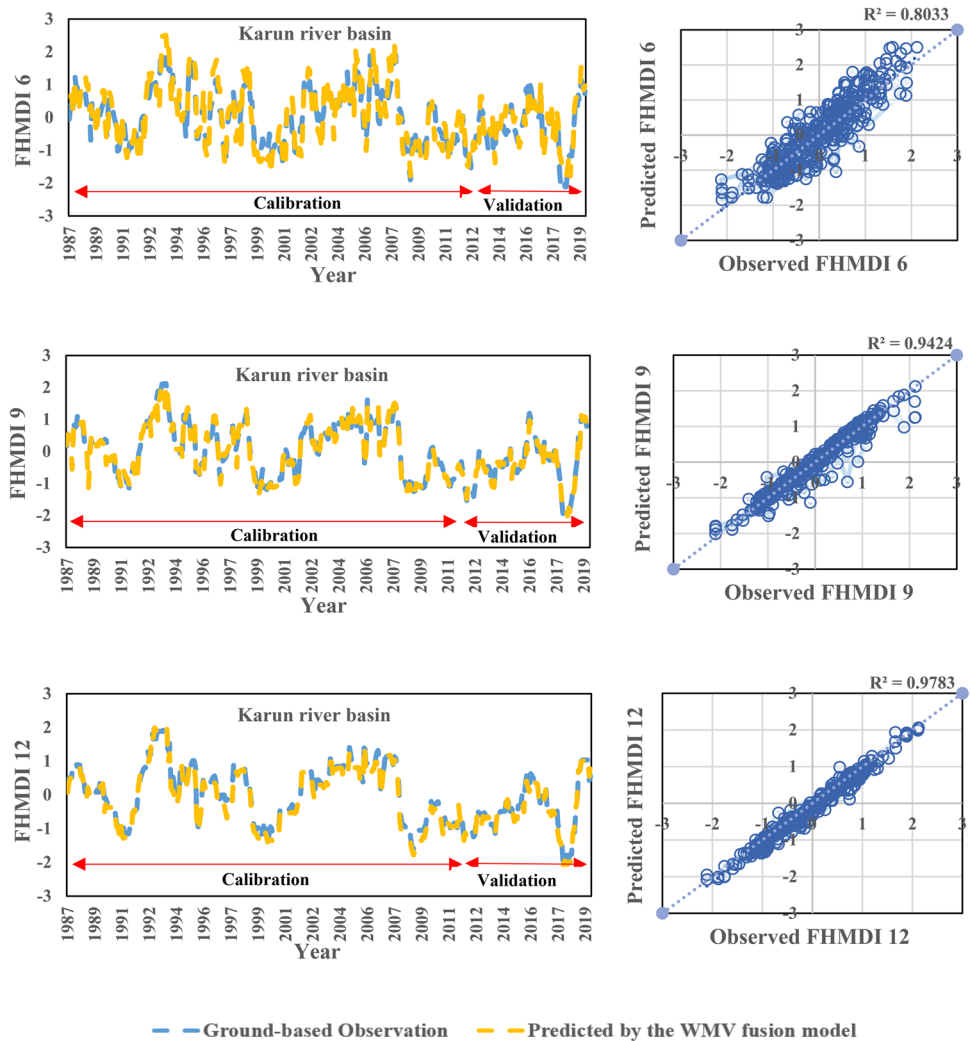
models to capture the complex relationships between meteorological and hydrological variables and drought occurrence. Among the various models used in research studies, the Gaussian Process Regression (GPR) model has demonstrated high performance in several research studies (Sihag et al. 2017; Mishra and Kushwaha 2019; Shabani et al. 2020; Ghasemi et al. 2021) similar to our results.

Our findings regarding the effectiveness of fusion-based models in accurately meteorological forecasting drought at different time scales are consistent with the results reported by Alizadeh and Nikoo (2018) and Fooladi et al. (2021). In other words, the fusion-based model application improved the accuracy of forecasting compared to all SAI models alone.

Conclusion

This study investigated four fusion-based methods for improving the accuracy of precipitation and runoff evaluation with low uncertainty and estimation of FHMDI using different remotely sensed precipitation and runoff products. In addition, the study compared the performance of single and composite products and single and composite models under different scenarios based on the four proposed fusion-based models using remotely sensed data versus ground-based FHMDI estimations at different timescales. The results indicated that while single products showed a good performance in some river basins, some fusion-based models improved the accuracy of dataset products compared to local measurements. However, the fusion-based assessment showed that fusing datasets did not perform satisfactorily in some river basins due to the high uncertainty of some single products. SAI models showed acceptable performance in composite drought prediction, especially at the 12-month timescale in clusters 1 and 2 under scenario 1. Fusion-based models significantly improved the accuracy of FHMDI estimation and research results compared to those of SAI models based on local measurement, especially in cluster 3. The WMV fusion-based method, with the lowest error, had a good performance in comparison with other products and

other SAI and fusion-based models. In addition, the estimation of FHMDI 12 had higher precision than FHMDI 6 as shown in other research. Overall, the WMV model was the best fusion framework with good performance in predicting FHMDI using remotely sensed datasets compared to ground observations, so it can be adopted as a reliable and accurate method for composite drought modeling.

Author contribution Mahnoosh Moghaddasi and Mehdi Mohammadi Ghaleni: conceptualization, methodology, technical investigation, writing, reviewing and editing, validation, visualization, supervision, software, technical investigation, data curation, and editing. Zaher Mundher Yaseen: writing up, editing, supervision, conceptualization, visualization. Fatemeh Moghaddasi: writing, original draft preparation, and preparing figures and tables.

Declarations

Ethics approval Not applicable, because this article does not contain any studies with human or animal subjects.

Consent to participate The research data were not prepared through a questionnaire.

Consent for publication There is no conflict of interest regarding the publication of this article.

Conflict of interest The authors declare no competing interests.

References

Abatzoglou JT, Dobrowski SZ, Parks SA, Hegewisch KC (2018) TerraClimate, a high-resolution global dataset of monthly climate and climatic water balance from 1958–2015. Sci Data 5:1–12

Ahmadebrahimpour E, Aminnejad B, Khalili K (2019) Assessment of the reliability of three gauged-based global gridded precipitation datasets for drought monitoring. Int J Glob Warm 18(2):103–119

Alam NM, Mishra PK, Jana C, Adhikary PP (2014) Stochastic model for drought forecasting for Bundelkhand region in Central India. Indian J Agric Sci 84:255–260

Alizadeh MR, Nikoo MR (2018) A fusion-based methodology for meteorological drought estimation using remote sensing data. Remote Sens Environ 211:229–247

Angelidis P, Maris F, Kotsovinos N, Hrissanthou V (2012) Computation of drought index SPI with alternative distribution functions. Water Resour Manag 26:2453–2473

Bacanli UG, Firat M, Dikbas F (2009) Adaptive neuro-fuzzy inference system for drought forecasting. Stoch Env Res Risk A 23(8):1143–1154

Balling RC, Keikhosravi Kiany MS, Sen Roy S, Khoshhal J (2016) Trends in extreme precipitation indices in Iran: 1951–2007. Adv Meteorol 1–8.

Barker LJ, Hannaford J, Chiverton A, Svensson C (2016) From meteorological to hydrological drought using standardised indicators. Hydrol Earth Syst Sci 20:2483–2505

Beck HE, Van Dijk AI, Levizzani V, Schellekens J, Miralles DG, Martens B, Roo AD (2017) MSWEP: 3-hourly 0.25 global gridded precipitation (1979–2015) by merging gauge, satellite, and reanalysis data. Hydrol Earth Syst Sci 21(1):589–615

Chen S, Gan TY, Tan X, Shao D, Zhu J (2019) Assessment of CFSR, ERA-Interim, JRA-55, MERRA-2, NCEP-2 reanalysis data for drought analysis over China. Clim Dyn 53:737–757

Crooks S, Kay A, Davies H, Bell V (2014) From catchment to national scale rainfall-runoff modelling: demonstration of a hydrological modelling framework. Hydrology 1(1):63–88

Dasarathy BV (1997) Sensor fusion potential exploitation-innovative architectures and illustrative applications. Proc IEEE 85:24–38

De Almeida R, Goh YM, Monfared R, Steiner MTA, West A (2020) An ensemble based on neural networks with random weights for online data stream regression. Soft Comput 24:9835–9855

Dee DP, Källén E, Simmons AJ, Haimberger L (2011) Comments on Reanalyses suitable for characterizing long-term trends. Bull Am Meteorol Soc 92:65–70

Dikshit A, Pradhan B (2021) Interpretable and explainable AI (XAI) model for spatial drought prediction. Sci Total Environ 801:149797

Dis MO, Anagnostou E, Mei Y (2016) Using high-resolution satellite precipitation for flood frequency analysis: case study over the Connecticut River Basin. J Flood Risk Manag 11:S514–S526

Docheshmeh Gorgij A, Alizamir M, Kisi O, Elshafie A (2022) Drought modelling by standard precipitation index (SPI) in a semi-arid climate using deep learning method: long short-term memory. Neural Comput & Applic 34:2425–2442

Ekbal A, Saha S (2011) Weighted vote-based classifier ensemble for named entity recognition. ACM Trans Asian Lang Inf Process 10:1–37

Ekbal A, Saha S (2012) Combining feature selection and classifier ensemble using a multiobjective simulated annealing approach: application to named entity recognition. Soft Comput 17:1–16

Fahimirad Z, Shahkarami N (2021) The impact of climate change on hydro-meteorological droughts using copula functions. Water Resour Manag 35:3969–3993

Farahmand A, AghaKouchak A (2015) A generalized framework for deriving nonparametric standardized drought indicators. Adv Water Resour 76:140–145

Fekete BM, Vörösmarty CJ, Grabs W (2002) High-resolution fields of global runoff combining observed river discharge and simulated water balances. Global Biogeochem Cycles 16:10–15

Feng P, Wang B, Liu DL, Yu Q (2019) Machine learning-based integration of remotely-sensed drought factors can improve the estimation of agricultural drought in South-Eastern Australia. Agric Syst 173:303–316

Fooladi M, Golmohammadi MH, Safavi HR, Singh VP (2021) Fusion-based framework for meteorological drought modeling using remotely sensed datasets under climate change scenarios: resilience, vulnerability, and frequency analysis. J Environ Manage 297:113283

Fooladi M, Golmohammadi MH, Rahimi I, Safavi HR, Nikoo MR (2023) Assessing the changeability of precipitation patterns using multiple remote sensing data and an efficient uncertainty method over different climate regions of Iran. Expert Syst Appl 221:119788

Ghasemi P, Karbasi M, Nouri AZ, Tabrizi MS, Azamathulla HM (2021) Application of Gaussian process regression to forecast multi-step ahead SPEI drought index. Alex Eng J 60(6):5375–5392

Ghiggi G, Humphrey V, Seneviratne SI, Gudmundsson L (2019) GRUN: an observation-based global gridded runoff dataset from 1902 to 2014. Earth Syst Sci Data 11(4):1655–1674

Ghiggi G, Humphrey V, Seneviratne SI, Gudmundsson L (2021) G-RUN ENSEMBLE: a multi-forcing observation-based global runoff reanalysis. Water Resour. Res.

Golian S, Javadian M, Behrangi A (2019) On the use of satellite, gauge, and reanalysis precipitation products for drought studies. Environ Res Lett 14:75005

Guttman NB (1999) Accepting the Standardized Precipitation Index: a calculation algorithm[1]. JAWRA J Am Water Resour Assoc 35:311–322

Hameed M, Ahmadalipour A, Moradkhani H (2018) Apprehensive drought characteristics over Iraq: results of a multidecadal spatiotemporal assessment. Geosciences 8(2):58

Hayes MJ, Svoboda MD, Wilhite DA, Vanyarkho OV (1999) Monitoring the 1996 drought using the Standardized Precipitation Index. Bull Am Meteorol Soc 80:429–438

Henriques AG, Santos MJJ (1999) Regional drought distribution model. Phys. Chem. Earth. Part B Hydrol Ocean Atmos 24:19–22

Hersbach H, Bell B, Berrisford P, Hirahara S, Horányi A, Muñoz-Sabater J, Nicolas J, Peubey C, Radu R, Schepers D (2020) The ERA5 global reanalysis. Q J R Meteorol Soc 146:1999–2049

Hosseini ZS, Moghaddasi M, Paimozd S (2023) Simultaneous monitoring of different drought types using linear and nonlinear combination approaches. Water Resour Manage 37(3):1125–1151

Hosseini-Moghari SM, Araghinejad S, Ebrahimi K (2018) Spatio-temporal evaluation of global gridded precipitation datasets across Iran. Hydrol Sci J 63:1669–1688

Huang S, Huang Q, Leng G, Liu S (2016) A nonparametric multivariate standardized drought index for characterizing socioeconomic drought: a case study in the Heihe River Basin. J Hydrol 542:875–883

Jalalkamali A, Moradi M, Moradi N (2015) Application of several artificial intelligence models and ARIMAX model for forecasting drought using the Standardized Precipitation Index. Int J Environ Sci Technol 12:1201–1210

Jiao J, Zhao M, Lin J, Ding C (2019) Deep coupled dense convolutional network with complementary data for intelligent fault diagnosis. IEEE Trans Ind Electron 66:9858–9867

Kaczmarek A, Rohm W, Klingbeil L, Tchórzewski J (2022) Experimental 2D extended Kalman filter sensor fusion for low-cost GNSS/IMU/Odometers precise positioning system. Measurement 193:110963

Kim H (2017) Global soil wetness project phase 3 atmospheric boundary conditions (experiment 1). Data Integr Anal Syst.

Knoben WJM, Freer JE, Woods RA (2019) Inherent benchmark or not? Comparing Nash-Sutcliffe and Kling-Gupta efficiency scores. Hydrol Earth Syst Sci 23:4323–4331

Kuswanto H, Naufal A (2019) Evaluation of performance of drought prediction in Indonesia based on TRMM and MERRA-2 using machine learning methods. MethodsX 6:1238–1251

Le MH, Kim H, Moon H, Zhang R, Lakshmi V, Nguyen LB (2020) Assessment of drought conditions over Vietnam using standardized precipitation evapotranspiration index, MERRA-2 reanalysis, and dynamic land cover. J Hydrol Reg Stud 32:100767

Li Q, Li P, Li H, Yu M (2014) Drought assessment using a multivariate drought index in the Luanhe River basin of Northern China. Stoch Environ Res Risk Assess 29:1509–1520

Li J, Zheng X, Zhang C, Deng X, Chen Y (2022) How to evaluate the dynamic relevance between landscape pattern and thermal environment on urban agglomeration? Ecol Indic 138:108795

Liu X, Zhu X, Zhang Q, Yang T, Pan Y, Sun P (2020) A remote sensing and artificial neural network-based integrated agricultural drought index: index development and applications. CATENA 186:104394

Marj AF, Meijerink AM (2011) Agricultural drought forecasting using satellite images, climate indices and artificial neural network. Int J Remote Sens 32:9707–9719

Mckee TB, Doesken NJ, Kleist J (1993) The relationship of drought frequency and duration to time scales. AMS 8th Conf Appl Climatol 22(17):179–183

Mishra AK, Desai VR (2005) Drought forecasting using stochastic models. Stoch Environ Res Risk Assess 19:326–339

Mishra AK, Desai VR (2006) Drought forecasting using feed-forward recursive neural network. Ecol Modell. https://doi.org/10.1016/j.ecolmodel.2006.04.017

Mishra N, Kushwaha A (2019) Rainfall prediction using gaussian process regression classifier. International Journal of Advanced Research in Computer Engineering & Technology (IJARCET) 8(8):392–397

Mishra AK, Singh VP (2010) A review of drought concepts. J Hydrol 391(1–2):202–216

Modaresi F, Araghinejad S, Ebrahimi K (2018) A comparative assessment of artificial neural network, generalized regression neural network, least-square support vector regression, and K-nearest neighbor regression for monthly streamflow forecasting in linear and nonlinear conditions. Water Resour Manag 32:243–258

Morid S, Smakhtin V, Moghaddasi M (2006) Comparison of seven meteorological indices for drought in Iran. Int J Climatol 26:971–985

Morid S, Smakhtin V, Bagherzadeh K (2007) Drought forecasting using artificial neural networks and time series of drought indices. Int J Climatol 27(15):2103–2111

Moshir Panahi D, Kalantari Z, Ghajarnia N, Seifollahi-Aghmiuni S, Destouni G (2020) Variability and change in the hydro-climate and water resources of Iran over a recent 30-year period. Sci Rep 10(1):7450

Motevali Bashi Naeini E, Akhoond-Ali AM, Radmanesh F, Koupai JA, Soltaninia S (2021) Comparison of the calculated drought return periods using tri-variate and bivariate copula functions under climate change condition. Water Resour Manag 35:4855–4875

Naderi K, Moghaddasi M, Shokri A (2022) Drought occurrence probability analysis using multivariate standardized drought index and copula function under climate change. Water Resour Manag 36:2865–2888

Nassaj BN, Zohrabi N, Shahbazi AN, Fathian H (2022) Evaluating the performance of eight global gridded precipitation datasets across Iran. Dyn Atmos Oceans 1(98):101297

Nazeri Tahroudi M, Ramezani Y, De Michele C, Mirabbasi R (2020) A new method for joint frequency analysis of modified precipitation anomaly percentage and streamflow drought index based on the conditional density of copula functions. Water Resour Manag 34:4217–4231

Nejatian N, Yavary Nia M, Yousefyani H, Shacheri F, Yavari Nia M (2023) The improvement of wavelet-based multilinear regression for suspended sediment load modeling by considering the physiographic characteristics of the watershed. Water Sci Technol 87(7):1791–1802

Nemati A, Najafabadi SHG, Joodaki G, Nadoushani SSM (2019) Spatiotemporal drought characterization using gravity recovery and climate experiment (GRACE) in the central plateau catchment of Iran. Environ Process 7:135–157

Nhi PTT, Khoi DN, Hoan NX (2018) Evaluation of five gridded rainfall datasets in simulating streamflow in the upper Dong Nai river basin. Vietnam Int J Digit Earth 12:311–327

Odon P, West G, Stull R (2019) Evaluation of reanalyses over British Columbia. Part II: daily and extreme precipitation. J Appl Meteorol Clim 58:291–315

Park S, Im J, Park S, Rhee J (2017) Drought monitoring using high resolution soil moisture through multi-sensor satellite data fusion over the Korean peninsula. Agric for Meteorol 237:257–269

Qi W, Liu J, Yang H, Zhu X, Tian Y, Jiang X, Huang X, Feng L (2020) Large uncertainties in runoff estimations of GLDAS versions 2.0 and 2.1 in China. Earth Sp Sci 7(1):1–11

Rahmat SN, Jayasuriya N, Bhuiyan MA (2017) Short-term droughts forecast using Markov chain model in Victoria, Australia. Theor Appl Climatol 129:445–457

Rahmati Ziveh A, Bakhtar A, Shayeghi A, Kalantari Z, Bavani AM, Ghajarnia N (2022) Spatio-temporal performance evaluation of 14 global precipitation estimation products across river basins in southwest Iran. J Hydrol Reg Stud 44:101269

Raziei T, Sotoudeh F (2017) Investigation of the accuracy of the European Center for Medium Range Weather Forecasts (ECMWF) in forecasting observed precipitation in different climates of Iran. J Earth Sp Phys 43(1):133–147

Rienecker MM, Suarez MJ, Gelaro R, Todling R, Bacmeister J, Liu E, Bosilovich MG, Schubert SD, Takacs L, Kim GK, Bloom S, Chen J, Collins D, Conaty A, da Silva AGuW, Joiner J, Koster RD, Lucchesi R, Molod A, Owens T, Pawson S, Pegion P, Redder CR, Reichle R, Robertson FR, Ruddick AG, Sienkiewicz M, Woollen J (2011) MERRA: NASA's modern-era retrospective analysis for research and applications. J Clim 24:3624–3648

Rodell M, Houser PR, Jambor U, Gottschalck J, Mitchell K, Meng CJ, Arsenault K, Cosgrove B, Radakovich J, Bosilovich M, Entin JK, Walker JP, Lohmann D, Toll D (2004) The global land data assimilation system. Bull Am Meteorol Soc 85(3):381–394

Saemian P, Hosseini-Moghari SM, Fatehi I, Shoarinezhad V, Modiri E, Tourian MJ, Sneeuw N (2021) Comprehensive evaluation of precipitation datasets over Iran. J Hydrol 603:127054

Saemian P, Tourian MJ, AghaKouchak A, Madani K, Sneeuw N (2022) How much water did Iran lose over the last two decades? J Hydrol Reg Stud 41:101095

Saha S, Moorthi S, Pan HL, Wu X, Wang J, Nadiga S, Tripp P, Kistler R, Woollen J, Behringer D (2010) Supplement: supplement to the NCEP climate forecast system reanalysis. Bull Am Meteorol Soc. 91:ES9–ES25

Sahoo RN, Dutta D, Khanna M, Kumar N, Bandyopadhyay SK (2015) Drought assessment in the Dhar and Mewat Districts of India using meteorological, hydrological and remote-sensing derived indices. Nat Hazards 77:733–751

Salio P, Hobouchian MP, García Skabar Y, Vila D (2015) Evaluation of high-resolution satellite precipitation estimates over southern South America using a dense rain gauge network. Atmos Res 163:146–161

Santos JF, Pulido-Calvo I, Portela MM (2010) Spatial and temporal variability of droughts in Portugal. Water Resour Res 46(3):W03503

Scanlon BR, Ruddell BL, Reed PM, Hook RI, Zheng C, Tidwell VC, Siebert S (2017) The food-energy-water nexus: transforming science for society. Water Resour Res 53:3550–3556

See L, Abrahart RJ (2001) Multi-model data fusion for hydrological forecasting. Comput & Geosci 27:987–994

Shabani S, Samadianfard S, Sattari MT, Mosavi A, Shamshirband S, Kmet T, Várkonyi-Kóczy AR (2020) Modeling pan evaporation using Gaussian process regression K-nearest neighbors random forest and support vector machines; comparative analysis. Atmosphere 11(1):66

Shen HW, Tabios GQ III (1995) Drought analysis with reservoirs using tree-ring reconstructed flows. J Hydraul Eng 121:413–421

Shu C, Burn DH (2004) Artificial neural network ensembles and their application in pooled flood frequency analysis. Water Resour Res 40(9):W09301

Shukla S, Wood AW (2008) Use of a standardized runoff index for characterizing hydrologic drought. Geophys Res Lett 35(2):1–7

Sihag P, Tiwari NK, Ranjan S (2017) Modelling of infiltration of sandy soil using gaussian process regression. Modeling Earth Systems and Environment 3:1091–1100

Sun Q, Miao C, Duan Q, Ashouri H, Sorooshian S, Hsu KL (2018) A review of global precipitation data sets: data sources, estimation, and intercomparisons. Rev Geophys h 56(1):79–107

Toride K, Cawthorne DL, Ishida K, Kavvas ML, Anderson ML (2018) Long-term trend analysis on total and extreme precipitation over Shasta Dam watershed. Sci Total Environ 626:244–254

Trambauer P, Maskey S, Winsemius H, Werner M, Uhlenbrook S (2013) A review of continental scale hydrological models and their suitability for drought forecasting in (sub-Saharan) Africa. Phys Chem Earth Parts a/b/c 66:16–26

Try S, Tanaka S, Tanaka K, Sayama T, Oeurng C, Uk S, Takara K, Hu M, Han D (2020) Comparison of gridded precipitation datasets for rainfall-runoff and inundation modeling in the Mekong River Basin. PLoS ONE 15:e0226814–e0226814

Ullah I, Ma X, Yin J, Asfaw TG, Azam K, Syed S, Liu M, Arshad M, Shahzaman M (2021) Evaluating the meteorological drought characteristics over Pakistan using in situ observations and reanalysis products. Int J Climatol 41:4437–4459

Wang L, Li X, Chen Y, Yang K, Chen D, Zhou J, Liu W, Qi J, Huang J (2016) Validation of the global land data assimilation system based on measurements of soil temperature profiles. Agric for Meteorol 218:288–297

Wu J, Chen X, Yao H, Gao L, Chen Y, Liu M (2017) Non-linear relationship of hydrological drought responding to meteorological drought and impact of a large reservoir. J Hydrol 551:495–507

Xing Z, Ma M, Su Z, Lv J, Yi P, Song W (2020) A review of the adaptability of hydrological models for drought forecasting. Proc Int Assoc Hydrol Sci 383:261–266

Xu L, Chen N, Moradkhani H, Zhang X, Hu C (2020) Improving global monthly and daily precipitation estimation by fusing gauge observations, remote sensing, and reanalysis data sets. Water Resources Research 56(3):e2019WR026444

Xu HP, Zhou YX, Sun YS, Li J, Haagmans RHN, Liu WS (2004) Wavelet and Spherical Wavelet Theories and their Applications in Potential Field. Science press, Beijing. (in Chinese)

Yan H, Moradkhani H, Zarekarizi M (2017) A probabilistic drought forecasting framework: a combined dynamical and statistical approach. J Hydro 548:291–304

J Yang J Chang Y Wang Y Li H Hu Che Y, ... Yao J, 2018 Comprehensive drought characteristics analysis based on a nonlinear multivariate drought index J Hydrol 557 651 667

Yuan F, Aliu O, Chung KC, Mahmoudi E (2017) Evidence-based practice in the surgical treatment of thumb carpometacarpal joint arthritis. J Hand Surg Am 42:104-112.e1

Yuan W, Liu M, Wan F (2019) Calculation of critical rainfall for small-watershed flash floods based on the HEC-HMS hydrological model. Water Resour Manag 33:2555–2575

Zhang D, Del Rio-Chanona EA, Petsagkourakis P, Wagner J (2019) Hybrid physics-based and data-driven modeling for bioprocess online simulation and optimization. Biotechnol Bioeng 116:2919–2930

Zhu J, Zhou L, Huang S (2018) A hybrid drought index combining meteorological, hydrological, and agricultural information based on the entropy weight theory. Arab J Geosci 11(5):1–12. https://doi.org/10.1007/s12517-018-3438-1